



HAL
open science

A cell fate decision map reveals abundant direct neurogenesis bypassing intermediate progenitors in the human developing neocortex

Laure Coquand, Clarisse Brunet Avalos, Anne-Sophie Macé, Sarah Farcy, Amandine Di Cicco, Marusa Lampic, Ryszard Wimmer, Betina Bessières, Tania Attie-Bitach, Vincent Fraisier, et al.

► **To cite this version:**

Laure Coquand, Clarisse Brunet Avalos, Anne-Sophie Macé, Sarah Farcy, Amandine Di Cicco, et al.. A cell fate decision map reveals abundant direct neurogenesis bypassing intermediate progenitors in the human developing neocortex. *Nature Cell Biology*, 2024, 26 (5), pp.698-709. 10.1038/s41556-024-01393-z . hal-04801814

HAL Id: hal-04801814

<https://hal.inrae.fr/hal-04801814v1>

Submitted on 25 Nov 2024

HAL is a multi-disciplinary open access archive for the deposit and dissemination of scientific research documents, whether they are published or not. The documents may come from teaching and research institutions in France or abroad, or from public or private research centers.

L'archive ouverte pluridisciplinaire **HAL**, est destinée au dépôt et à la diffusion de documents scientifiques de niveau recherche, publiés ou non, émanant des établissements d'enseignement et de recherche français ou étrangers, des laboratoires publics ou privés.

1
2 **A cell fate decision map reveals abundant direct neurogenesis**
3 **in the human developing neocortex**
4

5 Laure Coquand^{1*}, Clarisse Brunet Avalos^{1*}, Anne-Sophie Macé², Sarah Farcy¹, Amandine Di
6 Cicco¹, Marusa Lampic¹, Ryszard Wimmer¹, Betina Bessières³, Tania Attie-Bitach³, Vincent
7 Fraisier², Pierre Sens⁴, Fabien Guimiot⁵, Jean-Baptiste Brault¹, Alexandre Baffet^{1, 6, 7}

8
9 1- Institut Curie, PSL Research University, CNRS UMR144, Paris, France

10 2- UMR 144-Cell and Tissue Imaging Facility (PICT-IBiSA), CNRS-Institut Curie, Paris,
11 France.

12 3- UF Embryofœtopathologie, Hopital Necker-enfants malades, Paris, France

13 4- Institut Curie, PSL Research University, CNRS UMR168, Paris, France

14 5- UF de Fœtopathologie – Université de Paris et Inserm UMR1141, Hôpital Robert Debré,
15 Paris, France

16 6- Institut national de la santé et de la recherche médicale (Inserm)

17 7- alexandre.baffet@curie.fr

18 *These authors contributed equally

19
20 **Abstract**

21 The human neocortex has undergone strong evolutionary expansion, largely due to an
22 increased progenitor population, the basal radial glial (bRG) cells. These cells are responsible
23 for the production of a diversity of cell types, but the successive cell fate decisions taken by
24 individual progenitors remain unknown. Here, we developed a semi-automated live/fixed
25 correlative imaging method to map bRG cell division modes in early fetal tissue and cerebral
26 organoids. Through the live analysis of hundreds of dividing progenitors, we show that bRG
27 cells undergo abundant symmetric amplifying divisions, and frequent self-consuming direct
28 neurogenic divisions, bypassing intermediate progenitors. These direct neurogenic divisions are
29 more abundant in the upper part of the subventricular zone. We furthermore demonstrate
30 asymmetric Notch activation in the self-renewing daughter cells, independently of basal fiber
31 inheritance. Our results reveal a remarkable conservation of fate decisions in cerebral
32 organoids, supporting their value as models of early human neurogenesis.

33 **Introduction**

34 The human neocortex, composed of billions of neuronal and glial cells, is at the basis
35 of higher cognitive functions¹. Its evolutionary size expansion is particularly important in the
36 upper layers, leading to increased surface area and folding². This is largely due to progenitor
37 cells called basal radial glial cells (bRGs), also known as outer radial glial cells³⁻⁶. These cells
38 are highly abundant in humans - but rare in mice^{7,8} – and reside in the outer subventricular zone
39 (OSVZ) where they may contribute to the majority of supragranular neurons⁹.

40 bRG cells derive from apical (also known as ventricular) RG cells but have lost their
41 connection to the ventricular surface through a process resembling an epithelial-mesenchymal
42 transition (EMT) (Fig. 1a)^{10,11}. A major feature of bRG cells is the presence of an elongated
43 basal process along which newborn neurons migrate, though various morphologies have been
44 reported including the presence of an apical process that does not reach the ventricle¹². bRG
45 cells express various RG markers such as PAX6, Vimentin and SOX2, and undergo an unusual
46 form of migration called mitotic somal translocation (MST) which occurs shortly before
47 cytokinesis¹³. Consistent with a steady increase of the bRG cell pool during development, live
48 imaging experiments have documented their high proliferative potential^{4,5,12}. bRG cells are
49 believed to increase the neurogenic output of the cortex while providing extra tracks for radial
50 migration and tangential dispersion of neurons¹⁴.

51 Genomic analyses have revealed the transcriptional profile of bRG cells as well as the
52 cellular diversity in the human developing neocortex¹⁵⁻¹⁷. They highlighted the conservation of
53 cellular identities between fetal tissue and cerebral organoids, despite some degree of metabolic
54 stress¹⁸⁻²³. Such studies led to the identification of several human bRG-specific genes with
55 important roles in bRG cell generation and amplification^{16,24-26}. These methods nevertheless do
56 not allow to identify the cell fate decisions taken at the single progenitor level that lead to this
57 diversity^{27,28}. Indeed, the sequence of progenitor divisions cannot be predicted from their final
58 cellular output²⁹. Identifying these progenitor cell fate decision modes (i.e. the fate of two
59 daughter cells) is critical to understand how neurogenesis is regulated across species, and
60 affected in pathological contexts. Before gliogenic stages, bRG cells can, theoretically, undergo
61 several division modes: symmetric proliferative (two RG daughters), symmetric self-
62 consuming (two differentiating daughters), or asymmetric self-renewing divisions (one RG and
63 one differentiating daughter). Moreover, differentiating divisions can lead to the production of
64 a neuron (direct neurogenic division) or an intermediate progenitor (IP, indirect neurogenic
65 division).

66 Here, we developed a method to quantitatively map human bRG cell division modes.
67 Using a semi-automated live-fixed correlative imaging approach that enables bRG daughter
68 cell fate identification following division, in space and in time, we have established a map of
69 cell fate decisions in human fetal tissue and cerebral organoids. We observe a remarkable
70 similarity of division modes between the two tissues, and identify two remarkable behaviors:
71 abundant symmetric amplifying divisions, as well as frequent self-consuming direct neurogenic
72 divisions, suggesting an alternative route to the asymmetric self-renewing divisions which
73 dominate in mouse aRG cells. Within these asymmetrically dividing cells, we demonstrate that
74 basal process inheritance does not correlate with asymmetric NOTCH signaling and self-
75 renewal, and is a consequence rather than a cause of bRG cell fate.

76

77 **Results**

78 **Morphological identification of bRG cells**

79 To identify human bRG cell division modes using live imaging methods, we first
80 validated the identification of these cells based on morphological features. Human fetal pre-
81 frontal cortex tissues from Gestational Week (GW) 14-18 were stained for phospho-Vimentin,
82 which marks mitotic RG cells. Imaging within the SVZ revealed four different morphologies
83 for these cells: unipolar with a single apical process (not reaching the VZ), unipolar with a basal
84 process, bipolar with both an apical and a basal process, and cells with no visible process (Fig.
85 1b, c). Mitotic bipolar bRG cells always had a major thick process and a minor thin process,
86 which could be apical or basal (Fig. 1b, 2P). Overall, over 80% p-VIM+ cells displayed at least
87 one process, and 60% a basal process. All process-harboring p-VIM+ cells were also SOX2+,
88 while 20% of non-polarized p-VIM+ cells were negative for SOX2 (Fig. 1d).

89 We then explored bRG cell morphology in non-mitotic cells. We first validated bRG
90 identity by showing that they were positive for HOPX and SOX2 (RG cells), but negative for
91 EOMES (IPs), and HuC/D and NEUN (Neurons) (Extended Data Fig. 1a, b). Fetal brain slices
92 were infected with GFP-expressing retroviruses (RV) and stained for SOX2, EOMES, and
93 NEUN (Fig. 1e and Extended Data Fig. 1c, d). This analysis confirmed that over 80% of
94 SOX2+/EOMES-/NEUN- cells displayed apical and/or basal processes, while 20% were non-
95 polarized (Fig. 1f, g). Moreover, the majority of process-harboring cells were SOX2+/EOMES-/
96 NEUN-, and around 40% of non-polarized cells were SOX2+/EOMES-/NEUN- (Fig. 1h).
97 Therefore, human fetal bRG cells largely display elongated processes, though 20% are non-
98 polarized.

99 We next performed live imaging of GFP-expressing cells in fetal slices, focusing on
100 elongated bRG cells. Dividing cells had the same morphology as previously described in fixed
101 samples (Extended Data Fig. 1e). The majority of process-harboring cells performed MST,
102 though 25% performed stationary divisions (Fig. 1i, j and Supplementary Video 1). MST could
103 occur in the apical direction or the basal direction, depending on their shape. When bRG cells
104 had two processes, MST occurred in the dominant (thick) process (Fig. 1j).

105 Finally, we asked whether these morphological features were conserved in dorsal
106 forebrain organoids. Week 8-10 organoids were infected with RV and stained for the cell fate
107 marker SOX2, EOMES and NEUN, which revealed abundant SOX2+ bRG cells above the
108 ventricular zone (Fig. 1k and Extended Data Fig 1f, g). As in fetal tissue, the majority of
109 SOX2+/EOMES-/NEUN- cells displayed one or two elongated processes, and 20% were non-
110 polarized (Fig. 1l, m). It was not possible to unambiguously identify whether processes were
111 apical or basal, as bRG cells were often located between two lumens. The vast majority of
112 process-harboring cells, and around 40% of non-polarized cells, were SOX2+/EOMES-
113 /NEUN- (Fig. 1n). Live imaging confirmed these morphologies and indicated that the majority
114 of bRG cells performed MST (Fig. 1o and Extended Data Fig 1h). Therefore, the majority of
115 human bRG cells can be identified in live samples based on their elongated morphology and
116 ability to divide, which is conserved between fetal tissue and organoids.

117

118 **A semi-automated correlative imaging method to identify cell fate decisions.**

119 We next developed a method to identify the fate acquired by daughter cells following
120 progenitor cell division in cerebral organoids. We established a correlative imaging method
121 consisting in live imaging GFP-expressing progenitors and, following fixation and
122 immunostaining, assigning a fate to the live imaged cells (Fig. 2a). The identification of
123 corresponding cells between the live and fixed samples can be particularly challenging as the
124 tissue is complex and multiple slices are imaged in parallel in up to 4 dishes (60-70 videos per
125 acquisition). Moreover, slices rotate and even flip during the immunostaining process. We
126 therefore developed a computer-assisted method to automate the localization of the videos in
127 the immunostained samples (see methods). In brief, RV-infected tissue slices are live imaged
128 for 48 hours and, at the end of the movie, 4X brightfield images of the slices containing
129 positional information from each video are generated (Fig. 2b and Supplementary Video 2).
130 Slices are then fixed, stained for the cell fate markers SOX2, EOMES, and NEUN, and mosaic
131 (tiled) images of the entire slices are acquired. Both live and fixed images are automatically
132 segmented, paired, flipped and aligned. The position of each video is thereby obtained on the

133 immunostained images, leading to the identification of matching cells between the live and
134 fixed samples (Fig. 2b). Using this method, dividing bRG cells can be live imaged and the fate
135 of the two daughter cells identified (Fig. 2c and Supplementary Video 3). Daughter cell fate
136 was analyzed on average 30 hours after division. We noted that when a daughter cell
137 differentiated (e.g. into an EOMES+ IP), it often retained some expression of the mother cell
138 fate marker (SOX2), irrespective of the division mode (Fig. 2c). Expression of a novel fate
139 marker was on the contrary very rapid, with EOMES or NEUN being detected in daughter cells
140 that had divided 1-2 hours before the end of the movie (Extended Data Fig. 2a). Moreover,
141 putative IPs and migrating neurons can be live imaged and cell fate analyzed at the last
142 timepoint (Fig. 2d, e and Supplementary Videos 4, 5). Therefore, this semi-automated
143 correlative microscopy method allows the identification of cell fate markers in live imaged
144 cerebral organoids, in a highly reproducible and quantitative manner.

145

146 **A map of cell fate decisions in cerebral organoids**

147 To generate a map of progenitor division modes, we analyzed 1,101 dividing bRG cells,
148 in weeks 7 to 9 and 13 to 15 cerebral organoids, prior to the start of gliogenesis^{18,20} (Fig. 3a,
149 extended data Fig. 2b, c, and Supplementary Videos 6, 7, 8). We report the relative
150 probabilities, through time, of all possible division modes: generation of (a) 2 bRGs; (b) 2 IPs;
151 (c) 2 neurons; (d) 1 bRG and 1 IP; and (e) 1 bRG and 1 neuron (Fig. 3b for week 8, and extended
152 data Fig. 3 for all other stages). Notably, we never observe asymmetrically dividing bRG cells
153 generating one IP and one neuron. We first quantified the fraction of proliferative (amplifying)
154 divisions (leading to two SOX2+ cells) versus neurogenic divisions (leading to at least one
155 differentiating cell, EOMES+ or NEUN+). This analysis revealed a high rate of bRG cell
156 amplification, which increases between weeks 7 and 9, and decreases between weeks 13 and
157 15 (Fig. 3c). Within neurogenic divisions, different patterns could be observed. bRG cells
158 performed symmetric self-consuming divisions, leading to two differentiating cells, or
159 asymmetric self-renewing divisions, leading to one bRG cell and one differentiating cell. Self-
160 consuming divisions decreased between weeks 7 and 9 and increased between weeks 13 and
161 15 (Fig. 3d). In both types of neurogenic divisions (asymmetric or symmetric), bRG cells could
162 divide directly into neurons or indirectly, via the generation of IPs. Strikingly, we observed that
163 direct neurogenic divisions dominated in human bRG cells, indicating that the generation of
164 IPs is not a systematic differentiation trajectory in these cells (Fig. 3e). These divisions
165 decreased between weeks 7 and 9 and increased between weeks 13 and 15 (Fig. 3e).

166 We next modeled how these different modes of progenitor divisions affected their final
167 output (see methods). At each stage, we predicted the average number of bRG cells, IPs and
168 neurons generated from a single bRG cell, after four rounds of division, which corresponds to
169 approximately 1 week of development (Fig. 3f for week 8 and extended data Fig. 4a for all
170 other stages). At week 8, 1 bRG cell leads on average to the generation of 5,75 bRG cells, 1,21
171 IPs and 2,69 neurons, highlighting their strong self-amplification potential (Fig. 3f). Modeling
172 bRG output through time reveals that bRG amplification increases from stage 7 to 9 and
173 decreased from 13 to 15 (Fig 3g). Strikingly, this occurs at a relatively constant neurogenic rate
174 indicating that, at the single progenitor level, self-amplification varies but not the number of
175 differentiated cells produced. Finally, we tested how variations in cell fate decision probabilities
176 would affect their output. Reducing the rate of proliferative divisions by 20% in favor of
177 asymmetric self-renewing indirect divisions (1bRG + 1 IP) - the dominant division mode in
178 mouse aRG cells at neurogenesis onset – reduced the total production of bRG cells by 31%
179 after only 4 divisions (Extended data Fig. 4b). Overall, this analysis indicates that bRG cells
180 are highly proliferative and undergo important self-amplification. Upon differentiation, they
181 undergo frequent self-consuming terminal divisions, as well as abundant direct neurogenesis.

182

183 **A map of cell fate decisions in human fetal tissue**

184 We next adapted this correlative imaging method to human frontal cortex samples at
185 GW 14-18. While slices were substantially larger, the macro proved to be very efficient at
186 automatically identifying and aligning corresponding regions between the live and fixed
187 datasets, indicating that it can be used for any type of tissues (Fig. 4a, b). We analyzed the
188 division modes of 227 human fetal bRG cells, following 48-hour live imaging (Fig. 4c,
189 extended data Fig. 5a and Supplementary Video; 9, 10). We confirmed the rapid expression of
190 differentiation markers following cell division (Extended Data Fig. 5b). As in cerebral
191 organoids, the majority of bRG cells performed symmetric proliferative division, generating
192 two SOX2+ daughters (Fig. 4d, e). At GW18, we noted a decrease in neurogenic division in
193 favor of gliogenic divisions, indicating that the switch begins around this developmental time.
194 Within neurogenic divisions, we again observed abundant symmetric self-consuming divisions
195 that remained relatively constant (around 32% of all neurogenic divisions) (Fig. 4d, f). Finally,
196 we confirmed that direct neurogenic divisions are an abundant bRG cell division mode, which
197 again remained stable from GW14 to 18 (over 40% of all neurogenic divisions) (Fig. 4d, g).
198 We tested whether these cell fate decisions varied depending on bRG cell mitotic behaviors
199 (apical MST, basal MST or static division) but found no clear effect of this parameter (Extended

200 Data Fig. 5c). Overall, we find a strong conservation of division modes between human fetal
201 tissue and cerebral organoids, with the coexistence of asymmetric self-renewing progenitors –
202 as classically observed in mouse aRG cells – together with self-amplifying and self-consuming
203 neurogenic progenitors which represent an alternative route for neuronal generation.

204

205 **Increased direct neurogenesis in the basal part of the human fetal OSVZ**

206 The human OSVZ is extremely large (approximately 3 mm at GW17) and bRG cells
207 may therefore be exposed to different microenvironments depending on their position, which
208 may influence their division modes. Moreover, bRG cells progressively migrate through the
209 SVZ and have a different history depending on their position. We therefore explored whether
210 bRG division modes vary along the apico-basal axis in the human fetal brain. To test this, we
211 adapted the above-described macro to automatically record the position of each dividing bRG
212 cell within the tissue. Distance to the apical surface was measured at the time of cytokinesis.
213 We then plotted the different division modes depending on bRG cell position within the tissue.

214 The position of bRG cells along the apico-basal axis only had a very minor effect on
215 symmetric proliferative versus neurogenic division (Fig. 5a, b). Similarly, the rate of symmetric
216 self-consuming versus asymmetric self-renewing divisions was not significantly different (Fig.
217 5a, b). However, we observed a clear difference in the rates of direct versus indirect
218 neurogenesis, depending on the position in the tissue. Indeed, indirect neurogenic divisions
219 (EOMES+ cells) occurred on average 800 μm from the apical surface, while direct neurogenic
220 divisions (NEUN+ cells) occurred much more basally, 1,306 μm from the apical surface (Fig.
221 5a, b). These experiments could not be performed in cerebral organoids, as they display a much
222 smaller OSVZ. Overall, they demonstrate that dividing bRG cells undergo more direct
223 neurogenic divisions when located in the basal part of the fetal OSVZ.

224

225 **Basal process inheritance does not predict bRG fate upon asymmetric division**

226 The mechanism of bRG cell asymmetric division remains unknown. In mouse aRG
227 cells, growing evidence support the role of basal process inheritance in stem cell fate
228 maintenance³⁰⁻³². We therefore used our correlative imaging method to test whether process
229 inheritance correlates with bRG fate maintenance upon asymmetric division of human bRG
230 cells. We first live imaged 79 asymmetrically-dividing bRG cells (one bRG daughter – one
231 differentiating daughter) within week 8-10 cerebral organoids, and analyzed daughter cell fate
232 depending on process inheritance (Fig. 6a, b and Supplementary Videos 11, 12). In half of these
233 cells, process-inheriting daughters maintained a bRG fate but in the other half, process-

234 inheriting daughters differentiated (Fig. 6c, d). This was the case whether the asymmetric
235 divisions generated an IP or directly a neuron. These results suggest no role for process
236 inheritance in bRG fate upon asymmetric cell division in cerebral organoids. We next
237 performed a similar analysis in GW 14-17 human fetal brain tissue. We analyzed 82
238 asymmetrically dividing bRG cells and again found no correlation between basal process
239 inheritance and bRG cell fate (Fig. 6e, f and Supplementary Videos 13, 14): 52.4% of basal
240 process-inheriting daughters remained bRG cells, and 47.6% differentiated (Fig. 6g, h). We did
241 not observe any effect of the apical process on cell fate either (not shown). In support of these
242 results, SOX2⁺ daughter cells that did not inherit a process could be observed to regrow a novel
243 basal process after division (Extended Data Fig. 6 and Supplementary Video 15). Therefore, in
244 human bRG cells, the basal process appears to be a consequence, rather than a cause, of bRG
245 cell fate upon asymmetric division. Its presence during interphase may however participate in
246 long-term bRG fate maintenance.

247

248 **Notch signaling is active in bRG daughters, not in process-inheriting cells**

249 We next addressed why basal process inheritance correlates with stem cell fate in mouse
250 aRG cells but not in human bRG cells, using the cerebral organoid model. In aRG cells, it was
251 proposed that the basal process acts as an antenna for the reception of Notch signaling from the
252 surrounding cells, in particular neurons^{31,32}. We first validated the role of Notch signaling for
253 bRG cell self-renewal in cerebral organoids⁴. Following retroviral infection to deliver GFP,
254 slices were treated with the γ -secretase inhibitor DAPT – which blocks Notch signaling – for 2
255 days. Quantification revealed a depletion of GFP⁺ bRG cells in favor of IPs, but not of neurons
256 (Extended Data Fig 7a, b). Therefore, indirect neurogenesis is the default differentiation
257 pathway in the absence of Notch signaling. We next investigated Notch signaling in bRG
258 daughter cells, depending on process inheritance. As a readout, we analyzed the expression of
259 its downstream target HES1. In cerebral organoids, HES1 was strongly expressed in the VZ
260 where aRG cells are highly abundant and in a sparse manner in the SVZ, reflecting the SOX2⁺
261 bRG cell distribution (Fig. 7a). Week 8-11 organoid slices were live imaged for 48 hours,
262 stained for HES1, EOMES and NEUN, and processed through the correlative imaging protocol.
263 Cell fate was determined based on EOMES and NEUN expression, with double-negative cells
264 being identified as bRG cells. Out of 276 bRG cell, 186 performed symmetric proliferative
265 divisions, 53 asymmetric divisions, and 37 symmetric self-consuming divisions (Fig. 7b).
266 Consistent with its oscillatory behavior in RG cells³³, HES1 was only detected in a subset of
267 bRG cells, whether these cells were generated following symmetric or asymmetric divisions

268 (Fig. 7c, d and Supplementary Video 16). As expected, HES1 was never detected in
269 differentiating cells (n=90 cells) (Fig. 7d). In total, out of 276 live imaged bRG cells, we
270 identified 16 cells that divided asymmetrically, with detectable HES1 expression in daughter
271 cells (Fig. 7d). HES1 was always detected in the non-differentiating daughter (EOMES- and
272 NEUN-), supporting preferential Notch signaling in the self-renewing bRG daughter upon
273 asymmetric division (Fig. 7d). However, we found no correlation between HES1 expression
274 and process inheritance: 8 HES1-expressing cells inherited the basal process and 8 did not (Fig.
275 7e, f and Supplementary Video 17). These data further support that process inheritance does
276 not correlate with bRG cell fate, and that the basal process is not involved in differential Notch
277 signaling upon asymmetric division in bRG cells, as it is believed to be in aRG cells.

278

279 **Discussion**

280 bRG cells are key actors in the evolutionary expansion of the human brain, but the
281 sequence of events leading to their massive neuronal output is unknown. Using live/fixed
282 correlative imaging, we provide a map of their division modes at early – mostly pre-gliogenic
283 – stages. Identifying the precise cell fate decisions that lead to given neuronal outputs is critical
284 to understand the diversity of differentiation trajectories taken by bRG cells. In mice, aRG cells
285 undergo a precise switch in division modes at E12.5, from mostly symmetric amplifying
286 divisions to mostly asymmetric divisions generating one self-renewing aRG cell and one IP that
287 will divide once to generate two neurons³⁴⁻³⁶. Here we show that, at neurogenesis onset,
288 multiple bRG cell division modes co-exist, pointing to a more complex regulation in the human
289 cortex.

290 We observe that bRG amplification through symmetric cell divisions is dominant, and
291 in organoids increases from weeks 7 to 9 and decreases from 13 to 15. Modelling reveals that
292 this occurs at a constant rate of neurogenesis, indicating that, at each developmental stage,
293 single bRG cells produce an equal number of differentiated cells, irrespective of their self-
294 amplification level. At the population level however, the gradual increase in the total number
295 of bRG cells during development will lead to an increase in the production of differentiated cells.
296 These results suggest that neuronal production increases through development as a consequence
297 of the expanding pool of bRG cells, but not of increased neurogenic potential of single bRG
298 cells.

299 Our results indicate that, on top of asymmetric self-renewing divisions, bRG cells
300 undergo symmetric amplifying divisions and self-consuming divisions, pointing to an
301 alternative route for neuronal generation. Neurogenic divisions are frequently direct, bypassing

302 IP production. This represents another major difference with mouse aRG cells that largely rely
303 on IPs to amplify the neurogenic output. The evolution of cortical neurogenesis in amniotes is
304 regulated by the balance between direct and indirect neurogenesis³⁷. aRG cells in sauropsids
305 undergo direct neurogenesis, while mammals largely rely on indirect divisions in the
306 evolutionary more recent neocortex, a process associated with size expansion and regulated by
307 Robo signaling levels³⁷. We show that this rule does however not apply to bRG cells, in which
308 direct neurogenesis is common. aRG cells rely on IPs to amplify their neurogenic output, and
309 we hypostatize that this may occur because their own self-amplification is limited by spatial
310 constraints. They must indeed divide at the ventricular surface to precisely segregate their apical
311 junctions between daughters and maintain a proper neuroepithelial structure. Interkinetic
312 Nuclear Migration (INM) leads to the formation of a pseudostratified epithelium that allows an
313 increase in the aRG cell pool, but their amplification still reaches a physical limit³⁸⁻⁴⁰. bRG cells
314 on the other hand are not subject to this physical limitation and can amplify their own pool both
315 radially and tangentially. In this regard, IPs may be less relied upon to increase the neurogenic
316 output. Whether direct and indirect divisions ultimately lead to the formation of different
317 neuronal subtypes, as observed in aRG cells, remains to be tested³⁷.

318 Cerebral organoids have emerged as a powerful system to investigate human brain
319 development⁴¹⁻⁴³. To what degree they faithfully recapitulate fetal neurogenesis is however
320 important to monitor. Genomics studies have highlighted the similarity of transcriptional
321 profiles, though substantial metabolic stress has been reported in organoids¹⁸⁻²³. Here, we report
322 a high similarity of bRG cell division modes between organoids and fetal tissue. We note that
323 direct neurogenesis is slightly more abundant in organoids, which may reflect cell stage
324 differences or inherent limitations of the organoid model. Nevertheless, an advantage of
325 imaging approaches such as ours is that the organoid necrotic core (from where most stress
326 likely originates) can be avoided, focusing on the cortical-like lobes at the periphery of the
327 organoids. These cortical-like structures are however much thinner than in the fetal brain,
328 limiting the ability to probe how bRG cell position impacts their division modes, as performed
329 here in fetal tissue.

330 The molecular mechanism regulating asymmetrical division in RG cells has been a
331 matter of controversy. In aRG cells, increasing evidence support a role for the basal process in
332 cell fate, which correlates with Notch activation and self-renewal³⁰⁻³². We however do not
333 observe such a correlation in human bRG cells where Notch signaling is activated in the self-
334 renewing daughter irrespective of basal process inheritance. aRG somas are located in the
335 ventricular zone and their basal process extends through the cortex, contacting neurons from

336 which Notch-Delta signaling can be activated. bRG somas on the other hand are located in the
337 SVZ and both their daughter cells are in close proximity to neurons. Therefore, due to the bRG
338 cell microenvironment, it is consistent that their basal process does not confer differential Notch
339 signaling. Other factors, such as centriole age, mitochondrial dynamics, mitotic spindle
340 positioning or Sara endosomes are promising candidates⁴⁴⁻⁴⁶.

341 Descriptions of clonal relationships are a powerful means to understand cellular
342 diversity. Key to this is the identification of the cell fate decision branch points along lineages.
343 The semi-automated correlative imaging method enables to quantitatively measure progenitor
344 cell division modes in human cortical tissue. This will allow to probe neuronal subtype
345 generation or the switch to gliogenesis, through time and space, across species, and in
346 pathological contexts.

347

348

349 **Material and methods**

350 **Ethics statement:**

351 Human fetal tissue samples were collected with previous patient consent and in strict
352 observance of legal and institutional ethical regulations. The protocol was approved by the
353 French biomedical agency (Agence de la Biomédecine, approval number: PFS17-003).

354

355 **Data and code availability**

356 The live imaging and immunofluorescence data that support the findings of this study are
357 available from the corresponding author (alexandre.baffet@curie.fr) or from the first authors
358 (coquand.laure@gmail.com - clarisse.brunet@curie.fr) upon request. The
359 LiveFixedCorrelative code is available at

360 http://xfer.curie.fr/get/lhGgGtXKbHF/Codes_correlative.zip

361

362 **Human iPSC culture**

363 The feeder-independent iPSC cell line used for this study was a gift from Silvia Cappello
364 (Max-Planck Institute of Psychiatry - Munich). Cells were reprogrammed from NuFF3-RQ
365 human newborn foreskin feeder fibroblasts (GSC-3404, GlobalStel)⁴⁷. iPSC cells were cultivated
366 as colonies on vitronectin-coated B3 dishes, using mTser medium (STEMCELL Technologies).
367 Colonies were cleaned daily under a binocular stereo microscope (Lynx EVO, Vision
368 Engineering), by manually removing differentiated cells with a needle.

369

370 **Cerebral organoids culture**

371 Cerebral organoids were derived from human iPS cells, following a previously
372 published protocol ⁴². Day 0 to day 4: iPS colonies of 1-2 mm of diameter were detached with
373 pre-warmed collagenase (1mg/mL) for 45 min at 37°C. After the addition of 1 mL of mTser,
374 floating colonies were transferred with a cut tip into a 15 ml tube for two series of gentle
375 washing with medium 1 (DMEM-F12 without phenol red, 20% KOSR, 1X GlutaMAX, 1X
376 MEM-NEAA, 1X 2-Mercaptoethanol, Pen/Strep, 2µM Dorsomorphin, 2 µM A-83). Colonies
377 were subsequently distributed in an ultra-low attachment 6-well plate with 3 mL of medium 1
378 and cultivated at 37°C, 5% CO₂. Day 5-6: Half of medium 1 was replaced daily with medium
379 2 (DMEM-F12 without phenol red, 1X N2 supplement, 1X GlutaMAX, 1X MEM-NEAA,
380 Pen/Strep, 1 µM CHIR-99021, 1 µM SB-421542). Day 7-14: At day 7, EBs were embedded in
381 Matrigel diluted in medium 2 at a ratio of 2:1. Matrigel-EB mixture was then spread in an ultra-
382 low attachment dish and incubated at 37°C for 30 min to solidify (10-20 EBs per well). Finally,
383 medium 2 was gently added to the well, without disturbing the Matrigel patch. On day 14,
384 Matrigel was mechanically broken by pipetting with a 5 mL pipet and transferred into a 15 mL
385 tube for gentle washing. Organoids were suspended in medium 3 (DMEM-F12 without phenol
386 red, 1X N2 supplement, 1X b27 supplement, 1X GlutaMAX, 1X MEM-NEAA, 1X 2-
387 Mercaptoethanol, Pen/Strep, 2.5 µg/mL Insulin) and grown in ultra-low attachment 6-well
388 plates under agitation at 100 rpm (Digital Orbital Shaker DOS-10M from ELMi). Day 35 to
389 84: Starting from day 35, medium 3 was supplemented with diluted Matrigel (1:100) ⁴⁸.

390

391 **Infection of human fetal cortex and cerebral organoids**

392 Fresh tissue from human fetal cortex was obtained from autopsies performed at the Robert
393 Debré Hospital, and Necker enfants malades Hospital (Paris). Tissues came from spontaneous
394 miscarriages or pregnancy terminations due to kidney malformations. or A piece of pre-frontal
395 cortex was collected from one hemisphere, and transported on ice from the hospital to the lab.
396 The tissue was divided into smaller pieces and embedded 4% low-gelling agarose (Sigma)
397 dissolved in artificial cerebrospinal fluid (ACSF). Cerebral organoids (week 8-12) were
398 embedded in 3% low-gelling agarose. Gel blocks from both tissues were then sliced with a
399 Leica VT1200S vibratome (300 µm-thick slices) in ice-cold ACSF. Slices were infected with
400 a GFP coding retrovirus, diluted in DMEM-F12. After 2h of incubation, slices were washed
401 three times with DMEM-F12 and grown on Millicell cell culture inserts (Merck) in cortical
402 culture medium (DMEM-F12 containing B27, N2, 10 ng/ml FGF, 10 ng/ml EGF, 5% fetal

403 bovine serum and 5% horse serum) for up to 5 days for human fetal brain and 48h for cerebral
404 organoids. Medium was changed every day.

405

406 **Live imaging in cerebral organoids and human fetal cortex slices**

407 To follow bRG cell divisions for approximately 48h, we used the following approach. 48h after
408 infection (3-5 days for human fetal brain), slices were placed under the microscope by
409 transferring the culture inserts in a 35 mm FluoroDish (WPI) with 1 mL of culture medium
410 (DMEM-F12 containing B27, N2, 10 ng/ml FGF, 10 ng/ml EGF, 5% fetal bovine serum and
411 5% horse serum). Live imaging was performed on a spinning disk wide microscope equipped
412 with a Yokogawa CSU-W1 scanner unit to increase the field of view and improve the resolution
413 deep in the sample. The microscope was equipped with a high working distance (WD 6.9-8.2
414 mm) 20X Plan Fluor ELWD NA 0.45 dry objective (Nikon), and a Prime95B SCMOS camera.
415 Z-stacks of 80-100 μm range were taken with an interval of 4-5 μm , and maximum projections
416 were performed. Videos were mounted in Metamorph. Image treatments (maximum
417 projections, subtract background, Median filter, stackreg and rotation) were carried out on Fiji.
418 Figures were assembled with Affinity Designer.

419

420 **Immunostaining of brain slices**

421 Human fetal brain and cerebral organoid slices in culture were fixed in 4% PFA for 2 hours.
422 Slices were boiled in sodium citrate buffer (10 mM, pH 6) for 20 minutes and cooled down at
423 room temperature (antigen retrieval). Slices were then blocked in PBS-Triton 100X 0.3%-
424 donkey serum 2% at room temperature for 2 hours, incubated with primary antibody overnight
425 at 4°C in blocking solution, washed in PBS-Tween 0.05%, and incubated with secondary
426 antibody overnight at 4°C in blocking solution before final wash and mounting in
427 Aquapolymount. Mosaics (tile scans) of fixed tissue were acquired with a CFI Apo LWD
428 Lambda S 40X objective (WI NA 1.15 WD 0.61-0.59, Nikon).

429

430 **Live and fixed correlative microscopy analysis**

431 The correlative microscopy method enables to automatically pair and align live and fixed
432 samples, for cell-cell matching. The macro, based on ImageJ⁴⁹ and Matlab, enables automated
433 contouring of the slices, matching of the live and fixed samples based on their area and shape,
434 and alignment of the samples (rotation and flip if needed). This leads to the precise positioning
435 of the live imaged cells on the immunostained images. This method is described in detail in the

436 **Annex 1.**

437 **Mathematical model**

438 The model considers 3 different cell types: bRG cells are type A, IP are type B, and neurons are type C.
439 The number of each cell type after x division is written I_x (with $I=A, B, C$) and the probability of
440 producing a cell of type I and a cell of type J after a bRG division is written p_{ij} . The average number
441 of the different cell type after x division satisfies the recurrence relations:

$$442 \quad A_x = A_{x-1}(2p_{aa} + p_{ab} + p_{ac}), B_x = B_{x-1} + A_{x-1}(p_{ab} + 2p_{bb}), C_x \\ 443 \quad = C_{x-1} + A_{x-1}(p_{ac} + 2p_{cc})$$

444 Therefore, after x division, the average number of cells of each cell type are

$$445 \quad A_x = A_0 \bar{p}_a^x, B_x = A_0 \bar{p}_b \frac{\bar{p}_a^{x-1}}{\bar{p}_a - 1}, C_x = A_0 \bar{p}_c \frac{\bar{p}_a^{x-1}}{\bar{p}_a - 1},$$

446 with

$$447 \quad \bar{p}_a = 2p_{aa} + p_{ab} + p_{ac}, \bar{p}_b = p_{ab} + 2p_{bb}, \bar{p}_c = p_{ac} + 2p_{cc}.$$

448 The number of bRG cells increases exponentially with the number of division if $\bar{p}_a > 1$ and decreases
449 if $\bar{p}_a < 1$. In the former case, the ratio of non bRG to bRG cells reaches a constant value $\frac{IP+Neurons}{bRG} =$
450 $\frac{2-\bar{p}_a}{\bar{p}_a-1}$.

456 **Retrovirus production**

457 To improve transfection efficiency, we used the HEK-Phoenix-GP cell line that stably
458 expresses the packaging enzymes GAL and POL. Cells were plated in 3xT300 (dilution at 1:20)
459 and grown for 3 days to reach 70% of confluence in DMEM-GlutaMax medium, 10% FBS (50
460 mL/flask). At day 3, cells were transfected with envelope VSVG plasmid and transfer plasmid
461 (CAG-GFP or MSCV-IRES-GFP) using Lipofectamine 2000. The two plasmids were mixed
462 into 5.4 mL of OptiMEM medium (18 μ g E-plasmid / 49.5 μ g t-plasmid). 337.5 μ L of
463 Lipofectamine 2000 was diluted in 5.4 mL of OptiMEM medium and incubated 5 min at room
464 temperature. The DNA preparation was thoroughly mixed into the Lipofectamine preparation
465 and incubated for 30 min at room temperature. In the meantime, medium was changed by 30
466 mL of DMEM-Glutamax (without FBS) per T300 flask. 3.6 mL of the DNA-Lipofectamine
467 mixture was then added to each T300 flask and incubated for 5h in a 37°C incubator. After this
468 period, flasks were carefully transferred into an L3 lab and the medium was changed for 30 mL
469 of fresh DMEM-GlutaMAX, 10% FBS. At day 5, medium was harvested into 50 mL tubes and
470 replaced by 30 mL of fresh medium (samples were stored at 4°C). At day 6, medium was
471 harvested, pooled with Day 5 samples and spun-down to pellet cell debris (1300 rpm, 5 min at
472 4°C). Supernatant was then filtered using 0.22 μ m filter unit and divided into 6 Ultra-Clear tubs

473 (Beckman Coulter – Ref.344058). Tubes were ultra-centrifuged at 31000 G for 1h30 at 4°C.
474 Supernatant was removed, retroviruses were collected with multiple PBS washings and
475 transferred into a single new Ultra-Clear tub. Final ultra-centrifugation was performed (31000
476 G for 1h30 at 4°C), supernatant was carefully removed and the thin pellet of retroviruses was
477 suspended into 750 µL of DMEM-F12 medium, aliquoted (50 to 100 µL aliquots) and stored
478 at -80°C. Titer of the preparation was tested by infecting regular HEK cells at different dilution
479 and the percentage of GFP+ cells was measured by FACS.

480

481 **NOTCH inhibition experiments**

482 For Notch inhibition experiments, 250µm-thick organoid slices were infected with a GFP
483 expressing retrovirus as described above. After infection, slices were transferred to Millicell
484 cell culture inserts (Merck) and placed in a 6-well plate containing cortical culture medium
485 supplemented with 5µM of DAPT (Tocris, 2364). Culture medium was refreshed every day.
486 After 48 hours, organoid slices were fixed, and immunostaining was performed. Cortical
487 culture medium was supplemented with DMSO for the control condition.

488

489 **Expression constructs and antibodies**

490 The following plasmids were used in this study: CAG-GFP (a gift from Victor Borrell); MSCV-
491 IRES-GFP (Tannishtha Reya, Addgene 20672); VSVG (a gift from Philippe Benaroch).
492 Antibodies used in this study were mouse anti-SOX2 (Abcam Ab79351, 1/500), sheep anti-
493 EOMES (R&D Systems AF6166, 1/500), rabbit anti-NEUN (Abcam Ab177487, 1/500), chicken
494 anti-GFP (Abcam Ab13970, 1/500), mouse anti-pVimentin (Abcam Ab22651, 1/1000), rat anti-
495 HES1 (MBL D134-3, 1/500), rabbit anti-NeuroD2 (Abcam, ab104430, 1/500), mouse anti-
496 HuC/HuD (ThermoFisher Scientific, A-21271, 1/200), rabbit anti-HOPX (Proteintech, 11419-
497 1-AP, 1/500), mouse anti-S100β (Synaptic systems 287111, 1/500), mouse anti-OLIG2
498 (Millipore MABN50, 1/200).

499

500 **Acknowledgements**

501 We acknowledge Institut Curie, member of the French National Research Infrastructure France-
502 BioImaging (ANR10-INBS-04) and the Nikon BioImaging Center (Institut Curie, France). We
503 thank Fiona Francis (IFRM) and Xavier Morin for helpful discussions and critical reading of
504 the manuscript. L.C. was funded by the French ministry of research (MESRI). A-S.M. was
505 funded by the Labex Cell(n)Scale and CNRS. A.D.B. is an INSERM researcher. This work was

506 supported by the CNRS, I. Curie, the ANR (ANR-20-CE16-0004-01) and the Ville de Paris
507 “Emergences” program.

508

509 **Author contributions**

510 L.C. and C.B.A performed experiments, analyzed data and wrote the manuscript. A-S.M. coded
511 the LiveFixedCorrelative macro, S.F., A.D.C. and M.L. generated organoids, B.S, T.A-B. and
512 F.G. provided fetal tissue, V.F. assisted with imaging, P. S. generated the mathematical model,
513 J-B. B. designed the project, performed experiments and analyzed data, and A.D.B. designed
514 the project and wrote the manuscript.

515

516 **References**

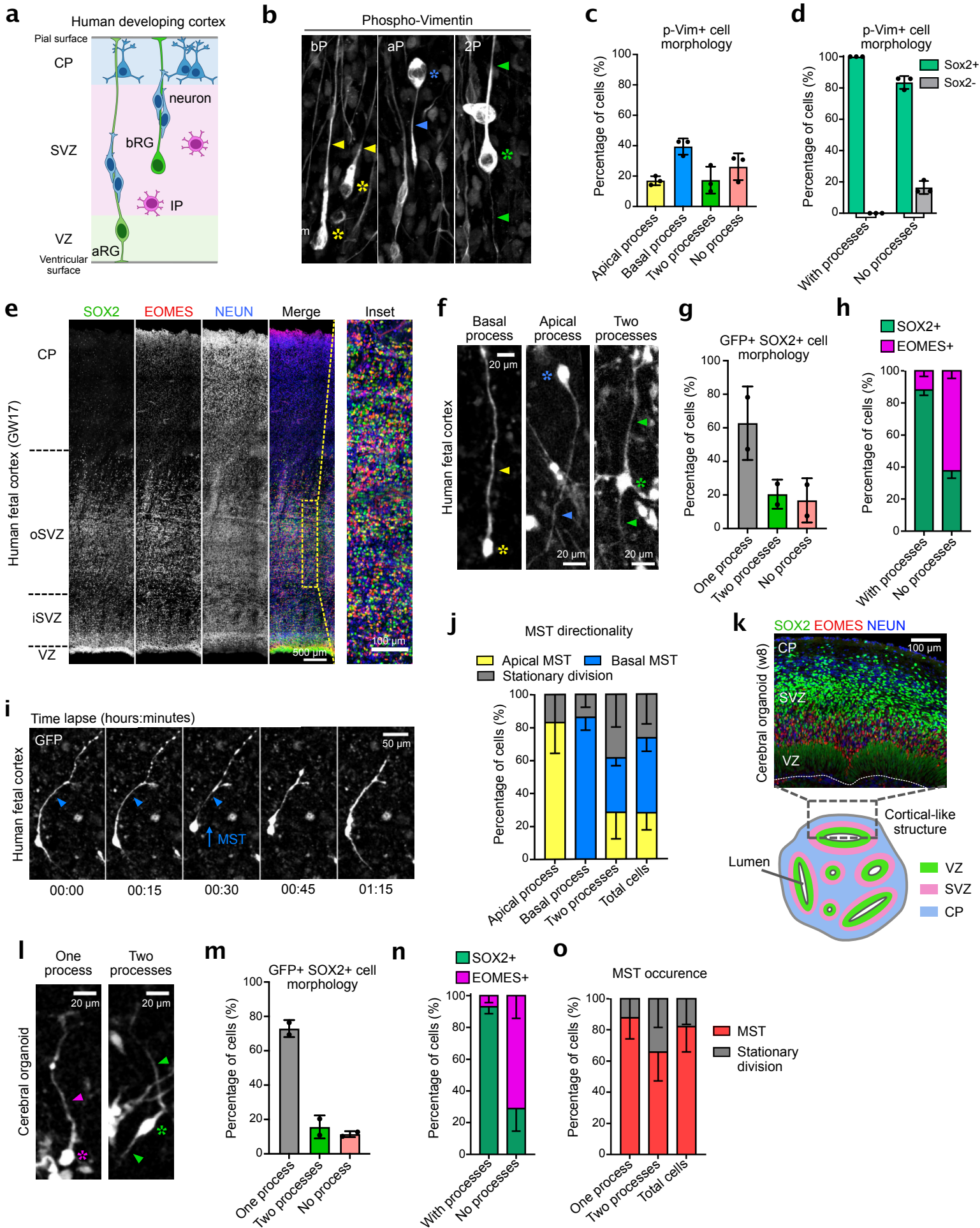
517

- 518 1. Cadwell, C. R., Bhaduri, A., Mostajo-Radji, M. A., Keefe, M. G. & Nowakowski, T. J.
519 Development and Arealization of the Cerebral Cortex. *Neuron* **103**, 980–1004 (2019).
- 520 2. Nowakowski, T. J., Pollen, A. A., Sandoval-Espinosa, C. & Kriegstein, A. R.
521 Transformation of the Radial Glia Scaffold Demarcates Two Stages of Human
522 Cerebral Cortex Development. *Neuron* **91**, 1219–1227 (2016).
- 523 3. Smart, I. H. M., Dehay, C., Giroud, P., Berland, M. & Kennedy, H. Unique
524 morphological features of the proliferative zones and postmitotic compartments of the
525 neural epithelium giving rise to striate and extrastriate cortex in the monkey. *Cereb.*
526 *Cortex* **12**, 37–53 (2002).
- 527 4. Hansen, D. V., Lui, J. H., Parker, P. R. L. & Kriegstein, A. R. Neurogenic radial glia in
528 the outer subventricular zone of human neocortex. *Nature* **464**, 554–561 (2010).
- 529 5. Fietz, S. A. *et al.* OSVZ progenitors of human and ferret neocortex are epithelial-like
530 and expand by integrin signaling. *Nat Neurosci* **13**, 690–699 (2010).
- 531 6. Reillo, I., De Juan Romero, C., García-Cabezas, M. Á. & Borrell, V. A role for
532 intermediate radial glia in the tangential expansion of the mammalian cerebral cortex.
533 *Cerebral Cortex* **21**, 1674–1694 (2011).
- 534 7. Wang, X., Tsai, J.-W., LaMonica, B. & Kriegstein, A. R. A new subtype of progenitor
535 cell in the mouse embryonic neocortex. *Nat Neurosci* **14**, 555–561 (2011).
- 536 8. Vaid, S. *et al.* A novel population of Hopx-dependent basal radial glial cells in the
537 developing mouse neocortex. *Development* **145**, dev169276–39 (2018).
- 538 9. Dehay, C., Kennedy, H. & Kosik, K. S. The outer subventricular zone and primate-
539 specific cortical complexification. *Neuron* **85**, 683–694 (2015).
- 540 10. LaMonica, B. E., Lui, J. H., Hansen, D. V. & Kriegstein, A. R. Mitotic spindle
541 orientation predicts outer radial glial cell generation in human neocortex. *Nature*
542 *Communications* **4**, 1665–11 (2013).
- 543 11. Martínez-Martínez, M. Á. *et al.* A restricted period for formation of outer
544 subventricular zone defined by Cdh1 and Trnp1 levels. *Nature Communications* **7**,
545 11812 (2016).
- 546 12. Betizeau, M. *et al.* Precursor diversity and complexity of lineage relationships in the
547 outer subventricular zone of the primate. *Neuron* **80**, 442–457 (2013).
- 548 13. Ostrem, B. E. L., Lui, J. H., Gertz, C. C. & Kriegstein, A. R. Control of outer radial
549 glial stem cell mitosis in the human brain. *CellReports* **8**, 656–664 (2014).

- 550 14. Fernández, V., Llinares-Benadero, C. & Borrell, V. Cerebral cortex expansion and
551 folding: what have we learned? *EMBO J* (2016). doi:10.15252/emboj.201593701
- 552 15. Pollen, A. A. *et al.* Molecular identity of human outer radial glia during cortical
553 development. *Cell* **163**, 55–67 (2015).
- 554 16. Florio, M. *et al.* Human-specific gene ARHGAP11B promotes basal progenitor
555 amplification and neocortex expansion. *Science* **347**, 1465–1470 (2015).
- 556 17. Nowakowski, T. J. *et al.* Spatiotemporal gene expression trajectories reveal
557 developmental hierarchies of the human cortex. *Science* **358**, 1318–1323 (2017).
- 558 18. Pollen, A. A. *et al.* Establishing Cerebral Organoids as Models of Human-Specific
559 Brain Evolution. *Cell* **176**, 743–756.e17 (2019).
- 560 19. Bhaduri, A. *et al.* Cell stress in cortical organoids impairs molecular subtype
561 specification. *Nature* **578**, 142–148 (2020).
- 562 20. Velasco, S. *et al.* Individual brain organoids reproducibly form cell diversity of the
563 human cerebral cortex. *Nature* **570**, 523–527 (2019).
- 564 21. Camp, J. G. *et al.* Human cerebral organoids recapitulate gene expression programs of
565 fetal neocortex development. *Proc Natl Acad Sci USA* **112**, 15672–15677 (2015).
- 566 22. Amiri, A. *et al.* Transcriptome and epigenome landscape of human cortical
567 development modeled in organoids. *Science* **362**, (2018).
- 568 23. Kanton, S. *et al.* Organoid single-cell genomic atlas uncovers human-specific features
569 of brain development. *Nature* **574**, 418–422 (2019).
- 570 24. Lui, J. H. *et al.* Radial glia require PDGFR- β signalling in human but not
571 mouse neocortex. *Nature* **515**, 264–268 (2014).
- 572 25. Fiddes, I. T. *et al.* Human-Specific NOTCH2NL Genes Affect Notch Signaling and
573 Cortical Neurogenesis. *Cell* **173**, 1356–1369.e22 (2018).
- 574 26. Suzuki, I. K. *et al.* Human-Specific NOTCH2NL Genes Expand Cortical Neurogenesis
575 through Delta/Notch Regulation. *Cell* **173**, 1370–1384.e16 (2018).
- 576 27. Gao, P. *et al.* Deterministic progenitor behavior and unitary production of neurons in
577 the neocortex. *Cell* **159**, 775–788 (2014).
- 578 28. He, Z. *et al.* Lineage recording in human cerebral organoids. *Nature methods* 1–10
579 (2021). doi:10.1038/s41592-021-01344-8
- 580 29. Fischer, E. & Morin, X. Fate restrictions in embryonic neural progenitors. *Current*
581 *Opinion in Neurobiology* **66**, 178–185 (2021).
- 582 30. Alexandre, P., Reugels, A. M., Barker, D., Blanc, E. & Clarke, J. D. W. Neurons derive
583 from the more apical daughter in asymmetric divisions in the zebrafish neural tube. *Nat*
584 *Neurosci* **13**, 673–679 (2010).
- 585 31. Shitamukai, A., Konno, D. & Matsuzaki, F. Oblique radial glial divisions in the
586 developing mouse neocortex induce self-renewing progenitors outside the germinal
587 zone that resemble primate outer subventricular zone progenitors. *Journal of*
588 *Neuroscience* **31**, 3683–3695 (2011).
- 589 32. Peyre, E. & Morin, X. An oblique view on the role of spindle orientation in vertebrate
590 neurogenesis. *Develop. Growth Differ.* **54**, 287–305 (2012).
- 591 33. Ochi, S., Imaizumi, Y., Shimojo, H., Miyachi, H. & Kageyama, R. Oscillatory
592 expression of Hes1 regulates cell proliferation and neuronal differentiation in the
593 embryonic brain. *Development* **147**, (2020).
- 594 34. Noctor, S. C., Martínez-Cerdeño, V., Ivic, L. & Kriegstein, A. R. Cortical neurons arise
595 in symmetric and asymmetric division zones and migrate through specific phases. *Nat*
596 *Neurosci* **7**, 136–144 (2004).
- 597 35. Haubensak, W., Attardo, A., Denk, W. & Huttner, W. B. Neurons arise in the basal
598 neuroepithelium of the early mammalian telencephalon: a major site of neurogenesis.
599 *Proc Natl Acad Sci USA* **101**, 3196–3201 (2004).

- 600 36. Miyata, T. *et al.* Asymmetric production of surface-dividing and non-surface-dividing
601 cortical progenitor cells. **131**, 3133–3145 (2004).
- 602 37. Huilgol, A. *et al.* Direct and indirect neurogenesis generate a mosaic of distinct
603 glutamatergic projection neuron in cerebral cortex. *Neuron* **111**, 2557-2569.e4 (2023).
- 604 38. Hu, D. J.-K. *et al.* Dynein recruitment to nuclear pores activates apical nuclear
605 migration and mitotic entry in brain progenitor cells. *Cell* **154**, 1300–1313 (2013).
- 606 39. Lee, H. O. & Norden, C. Mechanisms controlling arrangements and movements of
607 nuclei in pseudostratified epithelia. *Trends Cell Biol* **23**, 141–150 (2013).
- 608 40. Baffet, A. D., Hu, D. J. & Vallee, R. B. Cdk1 Activates Pre-mitotic Nuclear Envelope
609 Dynein Recruitment and Apical Nuclear Migration in Neural Stem Cells. *Dev Cell* **33**,
610 703–716 (2015).
- 611 41. Lancaster, M. A. *et al.* Cerebral organoids model human brain development and
612 microcephaly. *Nature* **501**, 373–379 (2013).
- 613 42. Qian, X. *et al.* Brain-Region-Specific Organoids Using Mini-bioreactors for Modeling
614 ZIKV Exposure. *Cell* **165**, 1238–1254 (2016).
- 615 43. Paşca, A. M. *et al.* Functional cortical neurons and astrocytes from human pluripotent
616 stem cells in 3D culture. *Nature methods* **12**, 671–678 (2015).
- 617 44. Wang, X. *et al.* Asymmetric centrosome inheritance maintains neural progenitors in the
618 neocortex. *Nature* **461**, 947–955 (2009).
- 619 45. Iwata, R., Casimir, P. & Vanderhaeghen, P. Mitochondrial dynamics in postmitotic
620 cells regulate neurogenesis. *Science* **369**, 858–862 (2020).
- 621 46. Kressmann, S., Campos, C., Castanon, I., Fürthauer, M. & González-Gaitán, M.
622 Directional Notch trafficking in Sara endosomes during asymmetric cell division in the
623 spinal cord. *Nat Cell Biol* **17**, 333–339 (2015).
- 624 47. Kyrousi, C. *et al.* Extracellular LGALS3BP regulates neural progenitor position and
625 relates to human cortical complexity. *Nature Communications* **12**, 6298–22 (2021).
- 626 48. Giandomenico, S. L. *et al.* Cerebral organoids at the air-liquid interface generate
627 diverse nerve tracts with functional output. *Nat Neurosci* **22**, 669–679 (2019).
- 628 49. Schindelin, J. *et al.* Fiji: an open-source platform for biological-image analysis. *Nature*
629 *methods* **9**, 676–682 (2012).
- 630

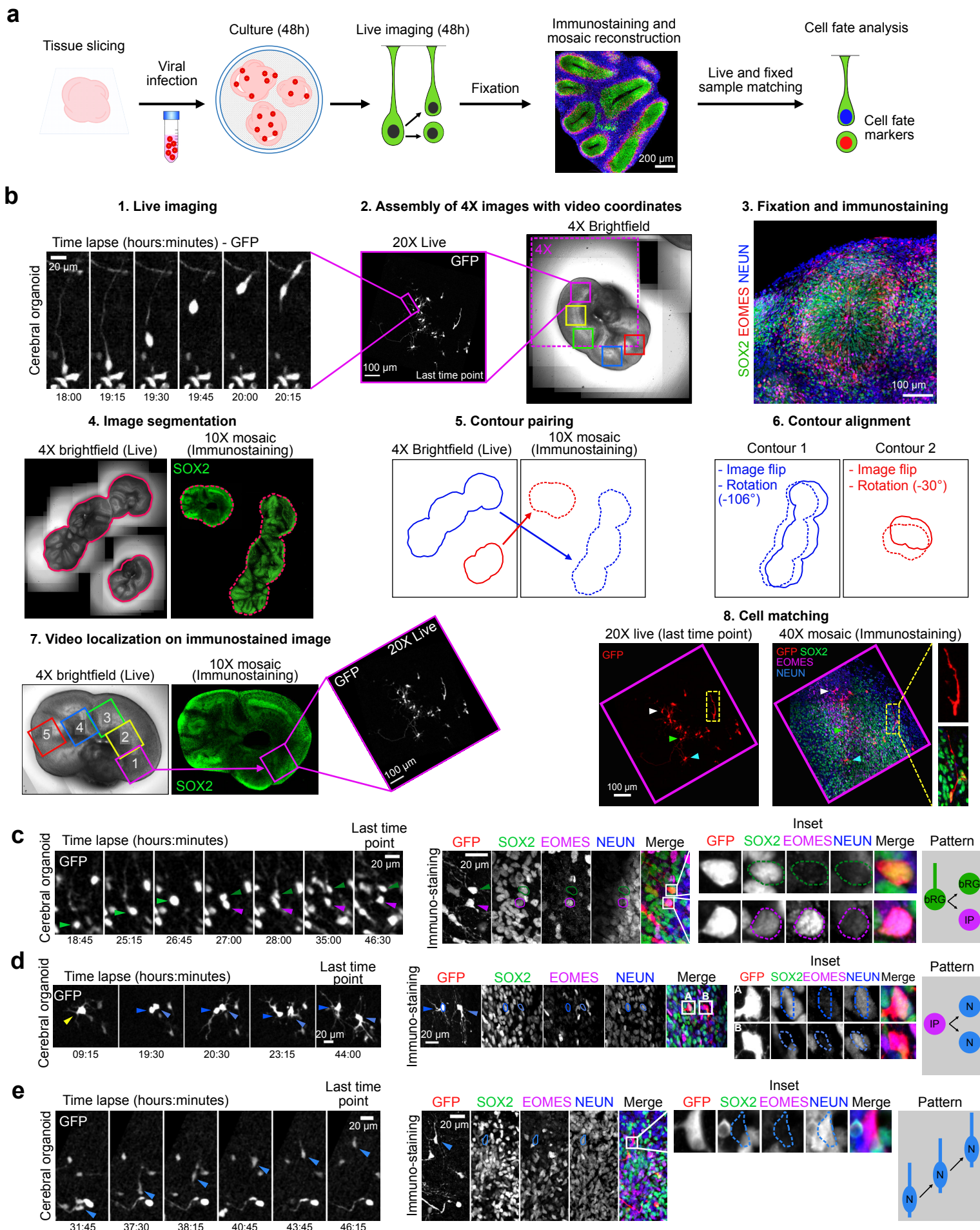
Figure 1



631 **Fig. 1 Morphological characterization of bRG cells in human cerebral organoids and fetal**
632 **tissue. a**, Schematic representation of human neocortex development. VZ: ventricular zone.
633 SVZ: subventricular zone. CP: cortical plate. aRG: apical radial glial progenitor. bRG: basal
634 radial glial progenitor. IP: Intermediate progenitor. **b**, Phospho-Vimentin immunostaining of
635 human frontal cortex at GW18. Image is overexposed to visualize processes, revealing cells
636 with basal process (bP), apical process (aP) and two processes (2P). Asterix indicate soma and
637 arrowheads indicate processes. **c**, Quantification of mitotic bRG cell morphologies in GW 14-
638 18 frontal cortex. (N=3 brains, 338 cells). **d**, Percentage of p-VIM+ cells positive for SOX2,
639 depending on morphology. (N=3 brains, 456 cells). **e**, SOX2, EOMES and NEUN
640 immunostaining in human frontal cortex at GW17. **f**, Morphologies of GFP-expressing SOX2+
641 cells in human frontal cortex at GW17. **g**, Quantification of morphologies of GFP expressing
642 SOX2+ cells in human frontal cortex at GW 14-17 (N=2 brains, 350 cells). **h**, Percentage of
643 SOX2+/EOMES- and EOMES+ (with or without SOX2) progenitors, depending on
644 morphology in human frontal cortex at GW 14-17 (N=2 brains, 204 cells). **i**, Live imaging of
645 bRG cell performing MST in human fetal tissue. Arrowhead indicates basal process. **j**,
646 Directionality of MST depending on bRG cell morphology in human frontal cortex at GW 14-
647 18 (N=3 brains, 242 cells). **k**, (Top) SOX2, EOMES and NEUN immunostaining in week 8
648 cerebral organoid. (Bottom) Schematic representation of week 8-10 cerebral organoids. **l**,
649 Morphologies of GFP expressing SOX2+ cells in cerebral organoids at weeks 7-10. **m**,
650 Quantification of morphologies of GFP-expressing SOX2+ cells in cerebral organoids at weeks
651 7-8. (N=2 batches, 104 cells) **n**, Percentage of SOX2+/EOMES- and EOMES+ (with or without
652 SOX2) progenitors, depending on morphology in cerebral organoids at weeks 8-10. (N=3
653 batches, 205 cells) **o**, Directionality of MST depending on bRG cell morphology cerebral
654 organoids at weeks 8-9 (N=4 batches, 260 cells). Error bars indicate SD.

655

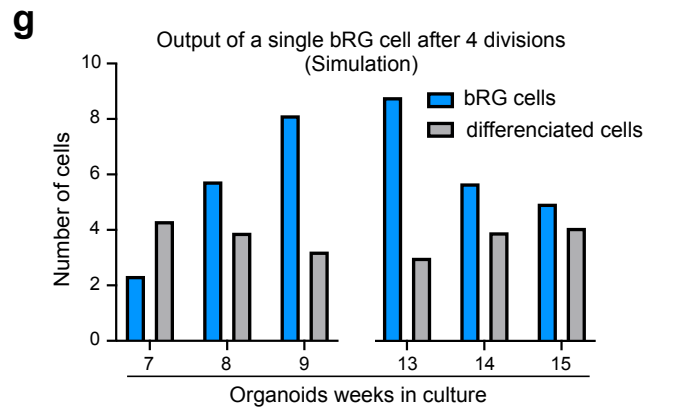
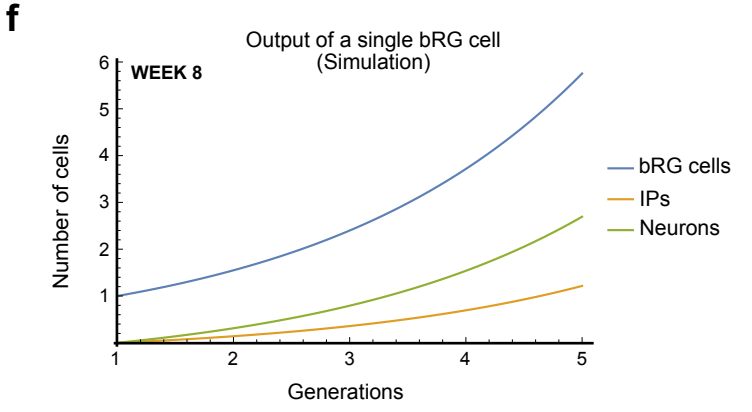
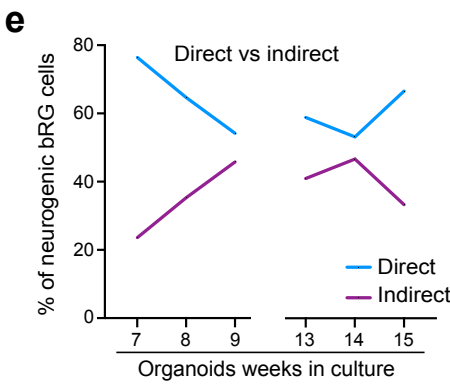
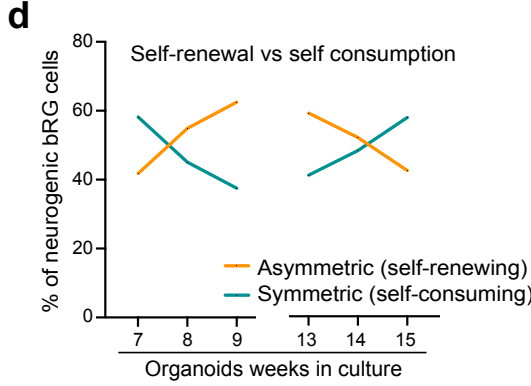
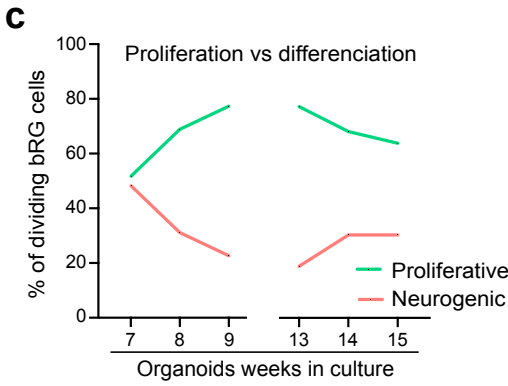
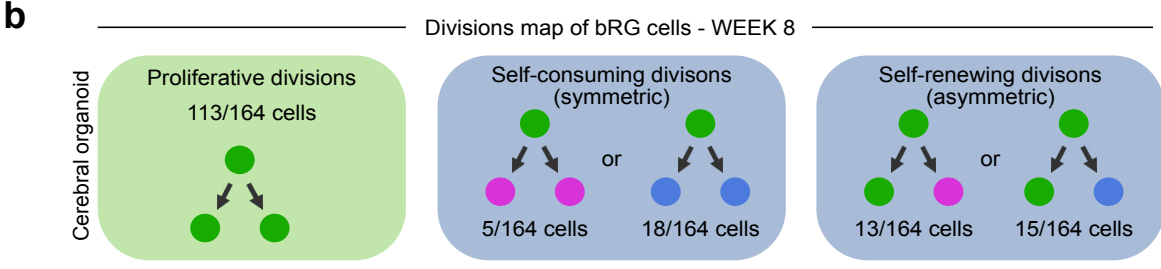
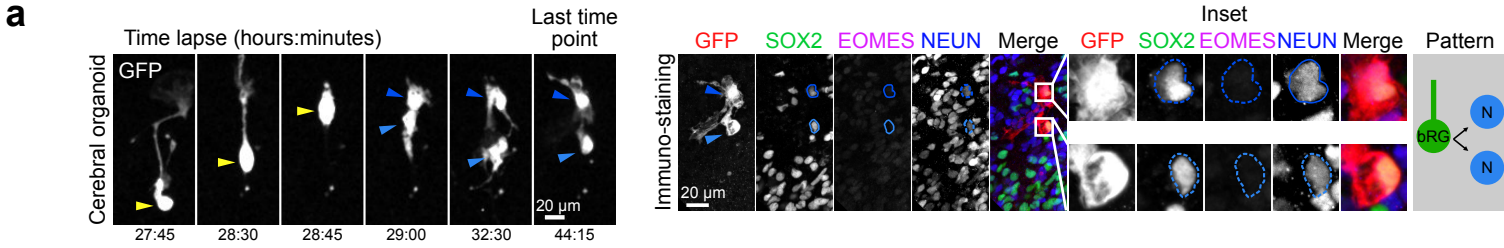
Figure 2



656 **Fig. 2 A semi-automated correlative imaging method to identify cell fate decisions in**
657 **cerebral organoids.**

658 **a**, Schematic representation of correlative microscopy pipeline. **b**, Step-by-step protocol for
659 semi-automated correlative microscopy. (1) bRG cells are live imaged for 48 hours. (2) 4X
660 brightfield images containing the video coordinates are assembled. (3) Organoid slices are
661 fixed, immunostained for SOX2, EOMES and NEUN and imaged. (4) Images are automatically
662 segmented to outline slices from live and fixed samples. (5) Slice contours are automatically
663 paired based on shape and area and (6) aligned (including a horizontal flip if needed). (7) Video
664 fields of view are automatically annotated on the immunostaining images. (8) Regions of
665 interest are re-imaged at higher resolution 40X and cells from live and fixed samples are
666 manually matched. **c**, Live/fixed correlative analysis of a dividing bRG cell generating a self-
667 renewing bRG daughter and a differentiating IP daughter. **d**, Live/fixed correlative analysis of
668 a dividing IP cell generating two neuronal daughters. **e**, Live/fixed correlative analysis of a
669 migrating neuron.
670

Figure 3

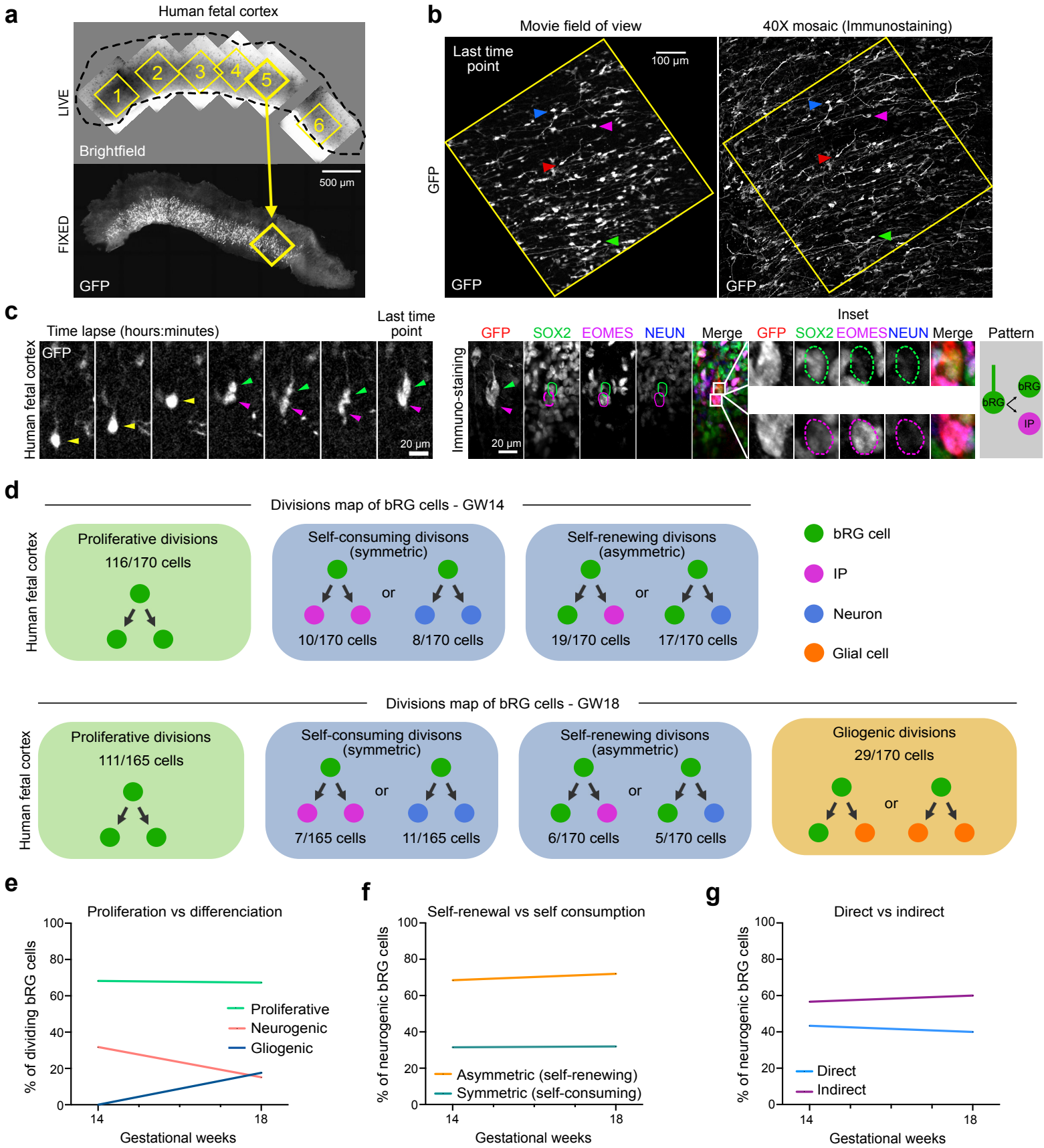


671 **Fig. 3 A map of cell fate decisions in human cerebral organoids.**

672 **a**, Live/fixed correlative analysis of a dividing bRG cell generating two neuronal daughters. **b**,
673 Summary of all division patterns identified in bRG cells in week 8 cerebral organoids (N=164
674 bRG cells). **c**, Percentage of proliferative versus neurogenic divisions of bRG cells in week 7-
675 9 and 13-15 cerebral organoids. **d**, Percentage of asymmetric (self-renewing) versus symmetric
676 (self-consuming) neurogenic divisions of bRG cells in week 7-9 and 13-15 cerebral organoids.
677 **e**, Percentage of direct versus indirect neurogenic divisions of bRG cells in week 7-9 and 13-
678 15 cerebral organoids. Week 7 (N=114 bRG cells), week 8 (N=164 bRG cells), week 9 (N=106
679 bRG cells), week 13 (N=206 bRG cells), week 14 (N=254 bRG cells) and week 15 (N=257
680 bRG cells) (**c-e**). **f**, Simulation of the output of a single bRG cell after 1-5 generations, based
681 on week 8 fate decision probabilities. **g**, Simulation of the output of a single bRG cell after 4
682 divisions (5 generations) in week 7-9 and 13-15 cerebral organoids.

683

Figure 4



684 **Fig. 4 A map of cell fate decisions in fetal human frontal cortex.**

685 **a**, Automated pairing of live and fixed samples and annotation of the video fields of view on
686 the immunostained fixed samples. **b**, GFP⁺ cell matching between the live images and the
687 fixed images. Arrowheads indicate equivalent cells. **c**, Live/fixed correlative analysis of a
688 dividing bRG cell generating a bRG daughter and an IP daughter. **d**, Summary of all division
689 patterns identified in bRG cells at GW 14 (N=170 bRG cells) and GW 18 (N=165 bRG cells)
690 human frontal cortex. **e**, Percentage of proliferative versus neurogenic divisions of bRG cells
691 in GW 14 and 18 human fetal tissue. **f**, Percentage of asymmetric (self-renewing) versus
692 symmetric (self-consuming) neurogenic divisions of bRG cells in GW 14 and 18 human fetal
693 tissue. **g**, Percentage of direct versus indirect neurogenic divisions of bRG cells in GW 14 and
694 18 human fetal tissue.

695

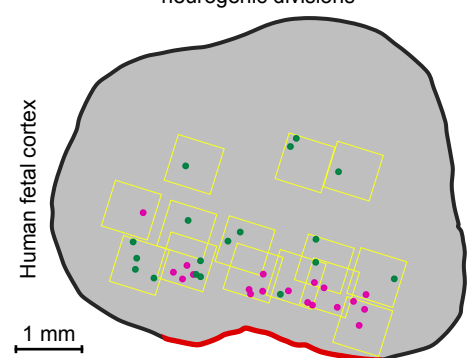
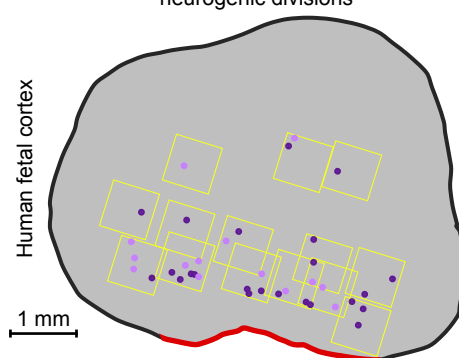
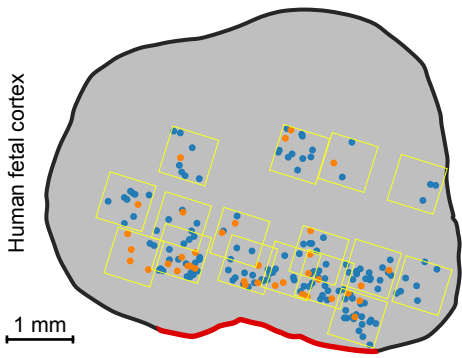
Figure 5

a

Proliferative versus neurogenic divisions

Self-consuming versus self-renewing neurogenic divisions

Direct versus indirect neurogenic divisions

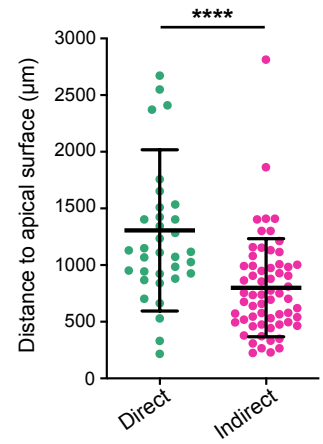
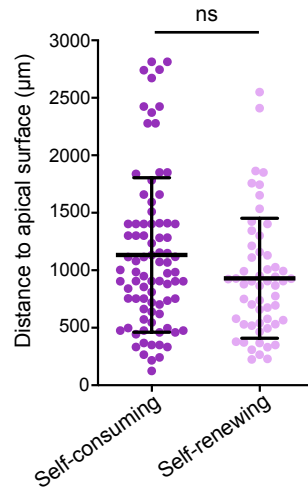
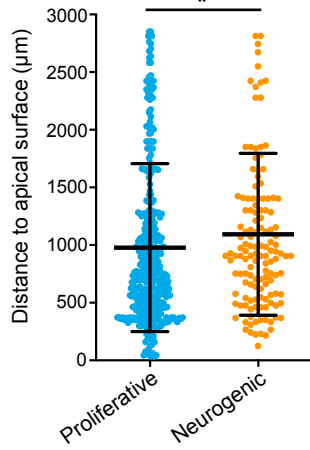


● Proliferative division ● Apical surface
● Neurogenic division ● 20X field of view

● Self-consuming division ● Apical surface
● Self-renewing division ● 20X field of view

● Direct neurogenesis ● Apical surface
● Indirect neurogenesis ● 20X field of view

b



696 **Fig. 5 Spatial distribution of division modes in human fetal cortex.**

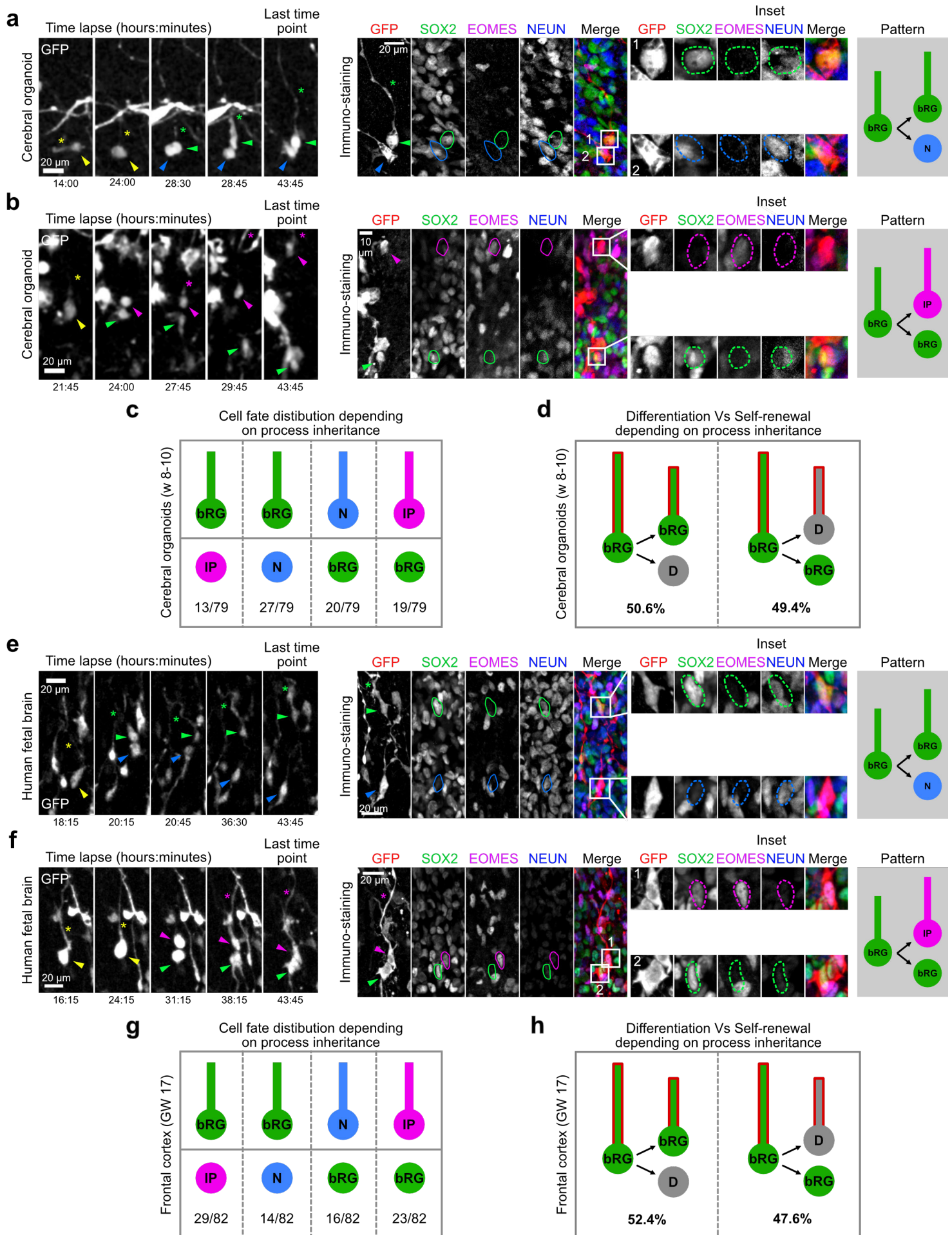
697 **a**, Spatial distribution of proliferative versus neurogenic, self-consuming versus asymmetric
698 self-renewing, and direct versus indirect neurogenic divisions in GW17 human frontal cortex.

699 **b**, Quantification of proliferative versus neurogenic, self-consuming versus asymmetric self-
700 renewing, and direct versus indirect neurogenic divisions in GW17-18 human frontal cortex.
701 (N=355 cells for GW17 and 172 cells for GW18). All data are expressed as mean +/- standard
702 deviation (SD). * $p < 0,05$, **** $p < 0,0001$ by two-tailed Mann-Whitney test.

703

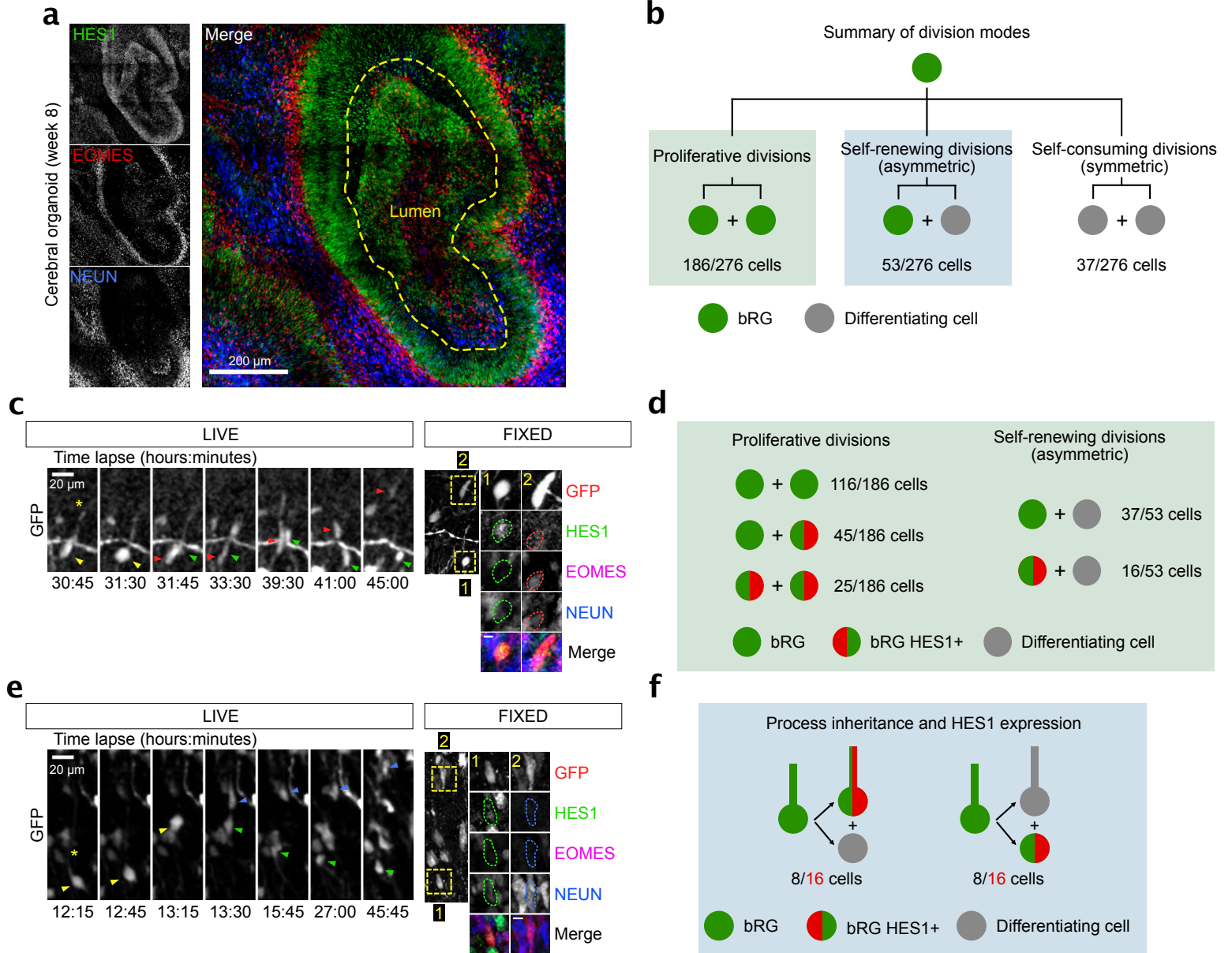
704

Figure 6



705 **Fig. 6 Basal process inheritance does not predict bRG fate upon asymmetric division.**
706 **a**, Live/fixed correlative analysis of basal process inheritance in a dividing bRG cell generating
707 a process-inheriting bRG daughter and neuron, within a cerebral organoid. **b**, Live/fixed
708 correlative analysis of basal process inheritance in a dividing bRG cell generating a process-
709 inheriting IP daughter and a bRG daughter, within a cerebral organoid. **c**, Distribution of cell
710 fates depending on process inheritance upon asymmetric cell division in week 8-10 cerebral
711 organoids (N=79 asymmetrically dividing cells from 5 experiments). **d**, Percentage of self-
712 renewing versus differentiating daughter cells upon asymmetric division, depending on process
713 inheritance in week 8-10 cerebral organoids (N=79 asymmetrically dividing cells from 5
714 experiments). **e**, Live/fixed correlative analysis of basal process inheritance in a dividing bRG
715 cell generating a process-inheriting bRG daughter and a neuron, within fetal frontal cortex. **f**,
716 Live/fixed correlative analysis of basal process inheritance in a dividing bRG cell generating a
717 process-inheriting IP daughter and a bRG daughter, within fetal frontal cortex. **g**, Distribution
718 of cell fates depending on process inheritance upon asymmetric cell division in GW 14-17
719 human frontal cortex (N=82 asymmetrically dividing cells from 2 experiments). **h**, Percentage
720 of self-renewing versus differentiating daughter cells upon asymmetric division, depending on
721 process inheritance in GW 14-17 human frontal cortex (N=82 asymmetrically dividing cells
722 from 2 experiments).
723

Figure 7

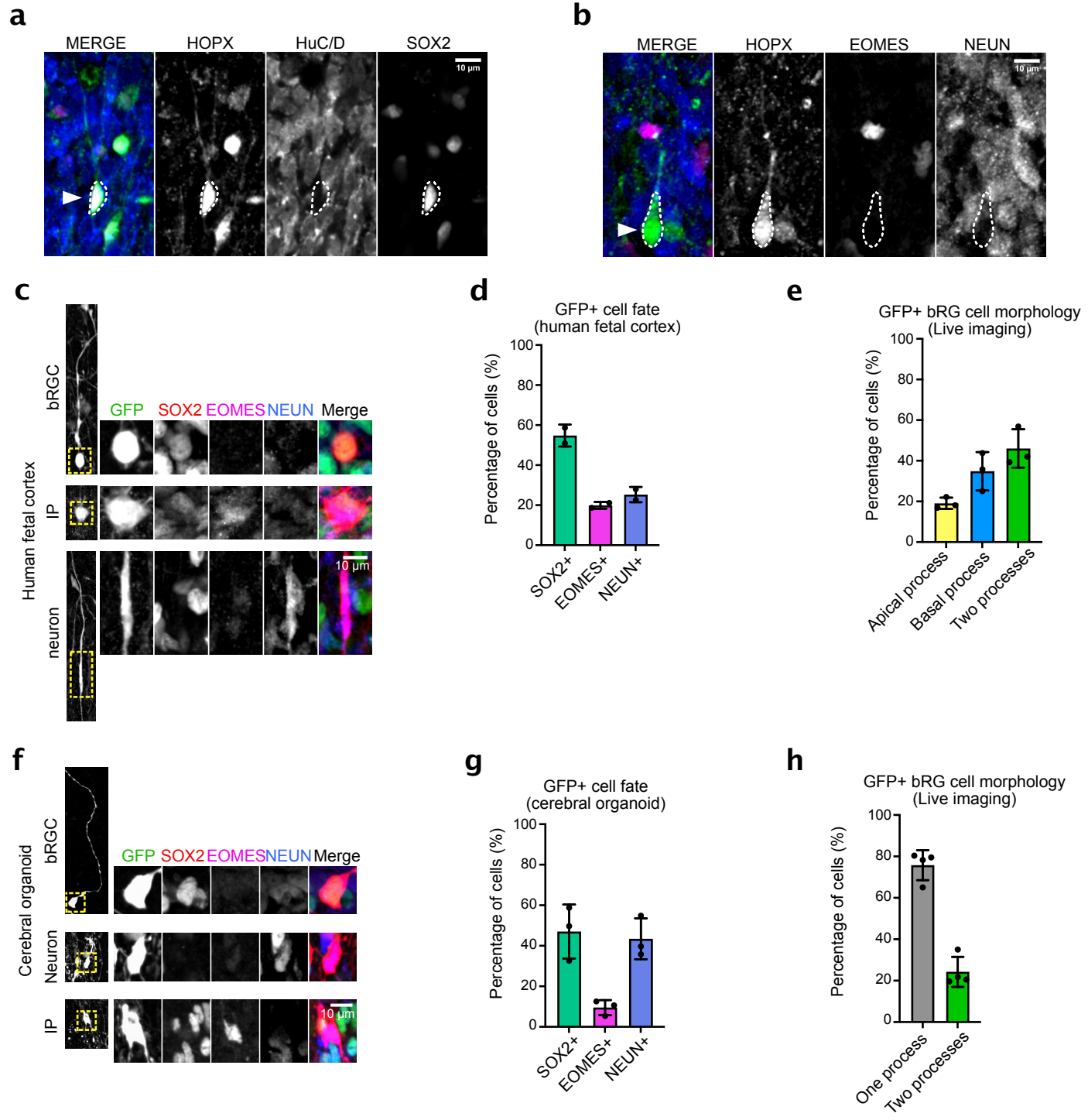


724 **Fig. 7 HES1 is preferentially expressed in bRG daughters, irrespective of process**
725 **inheritance.**

726 **a**, HES1, EOMES and NEUN immunostaining in human cerebral organoid at week 8. **b**,
727 Distribution of division modes identified in bRG cells within week 8-11 cerebral organoids.
728 bRG daughter (EOMES- and NEUN-), differentiating daughter (EOMES+ or NEUN+) (N=276
729 bRG cells from 3 batches of organoids). **c**, Live/fixed correlative analysis of an asymmetrically
730 dividing bRG cell revealing HES1 expression specifically in self-renewing daughter (EOMES-
731 and NEUN-). **d**, Summary of HES1 expression in daughter cells depending on division modes
732 (N= 239 cells from 3 batches of organoids). **e**, Live/fixed correlative analysis in asymmetrically
733 dividing bRG cells revealing lack of correlation between HES1 expression and basal process
734 inheritance. **f**, Summary of HES1 expression depending on process inheritance in
735 asymmetrically dividing bRG cells, within week 8-11 cerebral organoids (N= 16 cells from 3
736 batches of organoids).

737

Figure S1

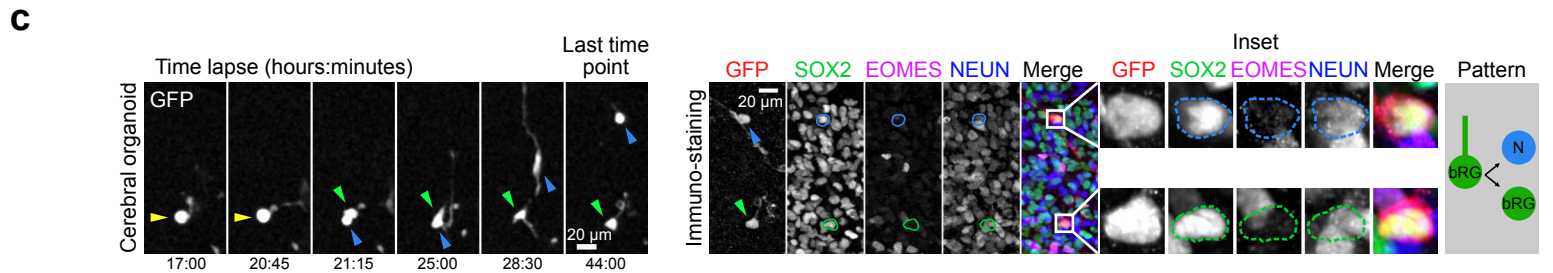
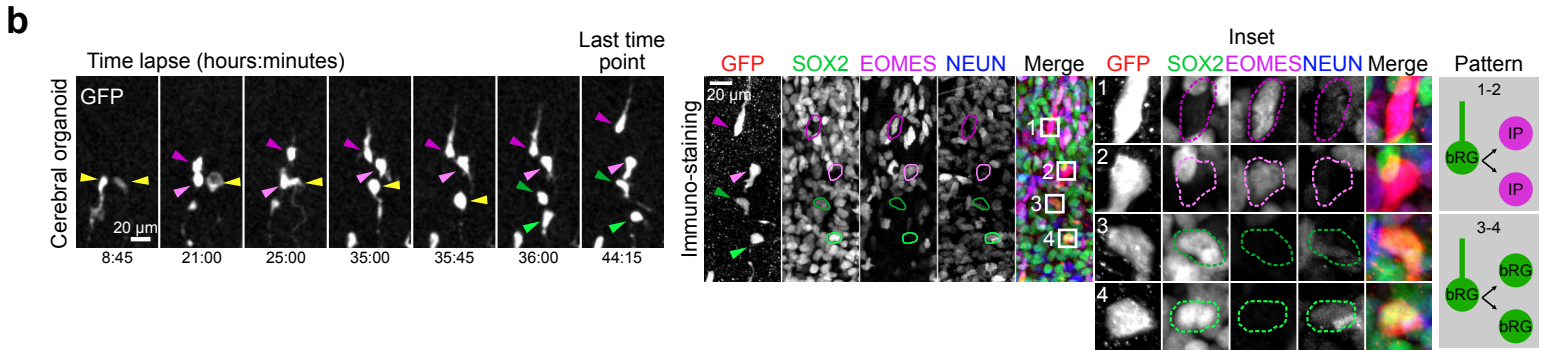
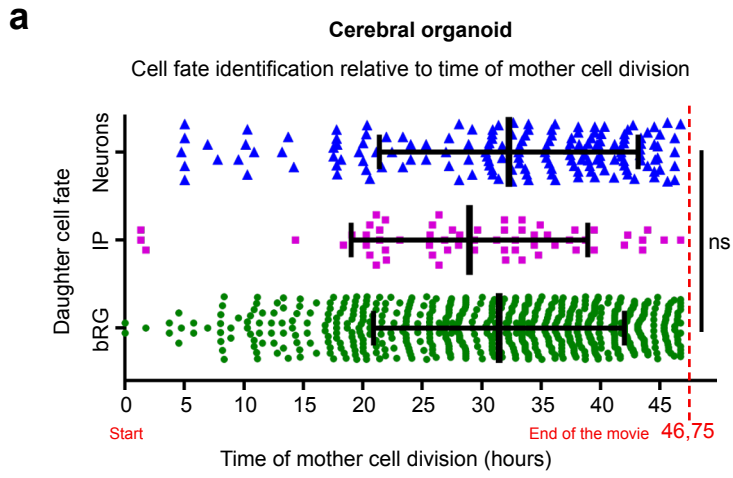


738 **Extended Data Fig. 1 Fate and shape of cells in cerebral organoids and fetal tissue.**

739 **a**, Immunostaining for HOPX, HuC/D and SOX2 in human fetal cortex at GW18. **b**,
740 Immunostaining for HOPX, EOMES and NEUN in human fetal cortex at GW18. **c**,
741 Immunostaining for SOX2, EOMES and NEUN in GFP-infected human fetal cortex at GW17.
742 **d**, Fate of GFP+ cells in human fetal cortex at GW 14-18. **e**, Morphology of GFP+ bRG cells
743 in live imaged human fetal samples at GW 14-18. **f**, Immunostaining for SOX2, EOMES and
744 NEUN in GFP-infected cerebral organoids at week 8. **g**, Fate of GFP+ cells in cerebral
745 organoids at week 8-10. **h**, Morphology of GFP+ bRG cells in live imaged cerebral organoids
746 at week 8-10.

747

Figure S2

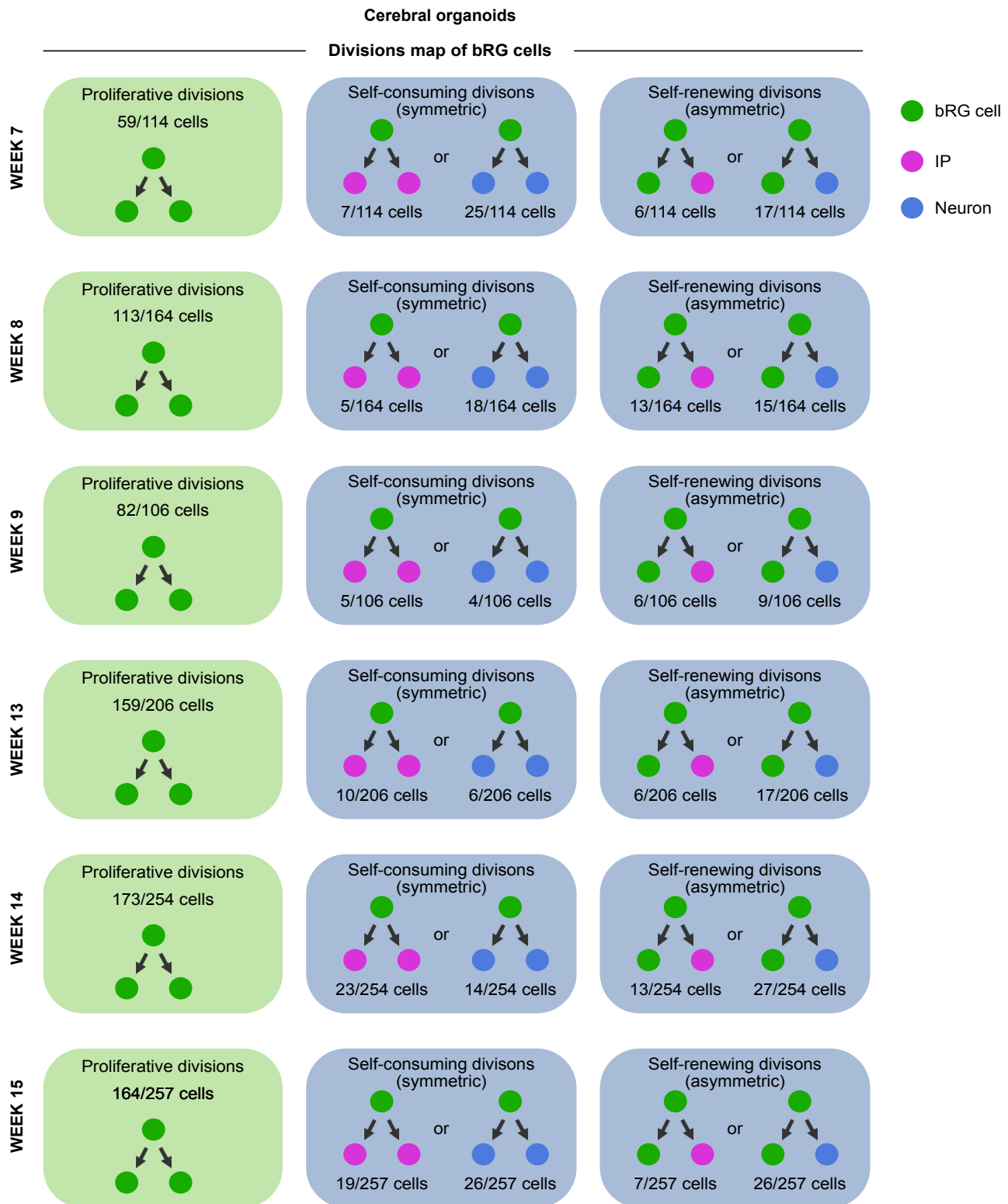


748 **Extended Data Fig. 2 Live/fixed correlative examples and cell fate identification timing in**
749 **cerebral organoids.**

750 **a**, Detection of bRG, IP or neuronal cell fate relative to the time of division of the bRG mother
751 cell in cerebral organoids at week 8-10. **b**, (Top) Live/fixed correlative analysis of a dividing
752 bRG cell generating two IP daughters. (Bottom). Live/fixed correlative analysis of a dividing
753 bRG cell generating two bRG daughters. **c**, Live/fixed correlative analysis of a dividing bRG
754 cell generating a bRG daughter and a neuronal daughter.

755

Figure S3



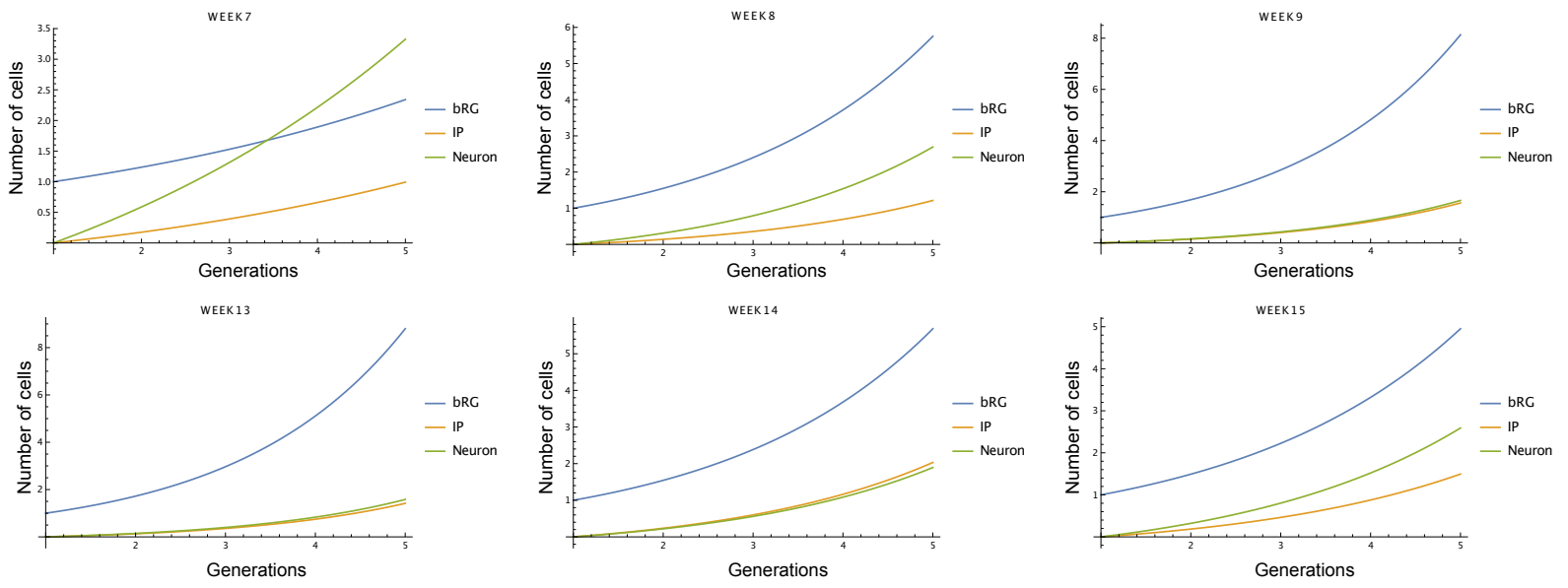
756 **Extended Data Fig. 3 Cell fate decision patterns in W7-15 cerebral organoids.**

757 Summary of all division patterns identified in bRG cells in week 7, 8, 9, 13, 14 and 15 cerebral
758 organoids. Week 7 (N=114 bRG cells), week 8 (N=164 bRG cells), week 9 (N=106 bRG cells),
759 week 13 (N=206 bRG cells), week 14 (N=254 bRG cells) and week 15 (N=257 bRG cells).

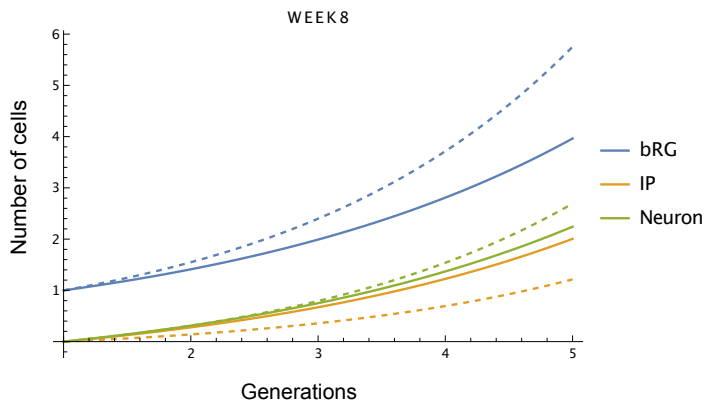
760

Figure S4

a



b



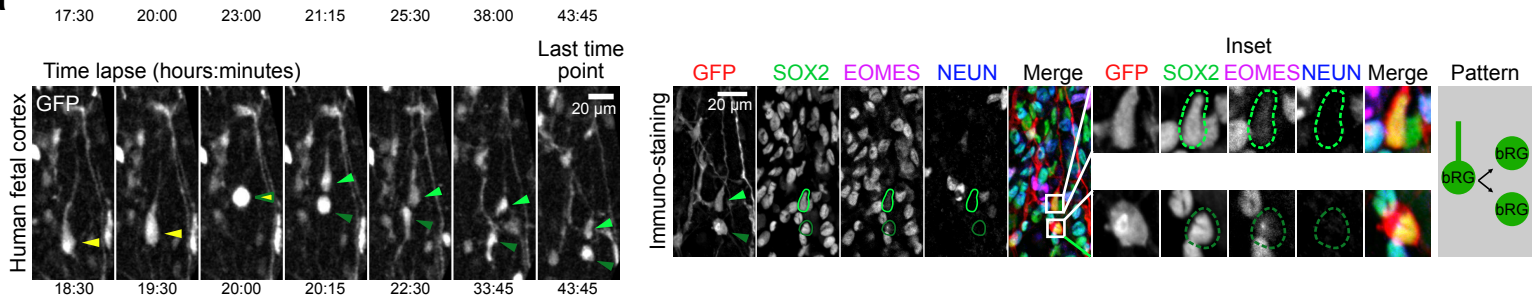
761 **Extended Data Fig. 4 bRG cells output in week 7-15 cerebral organoids.**

762 **a**, Simulation of the output of a single bRG cell after 1-5 generations, in week 7-9 and 13-15
763 cerebral organoids. **b**, Simulation of the output of a single bRG cell after 1-5 generations in
764 week 8 cerebral organoids (dashed lines) compared to the output of a single bRG cell that
765 underwent 20% less symmetric amplifying divisions in favor of asymmetric indirect divisions
766 (full lines).

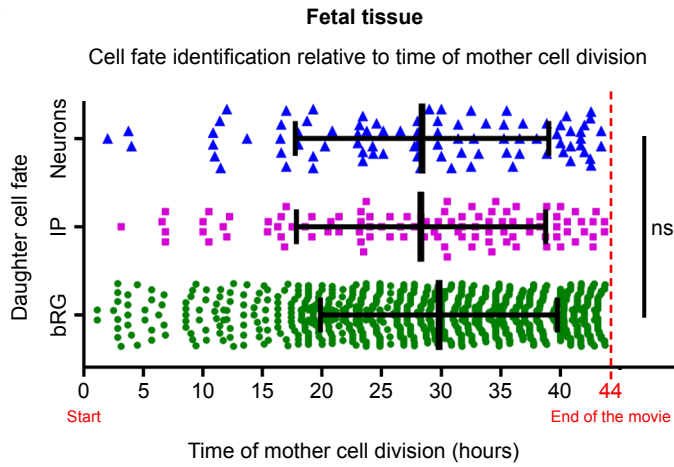
767

Figure S5

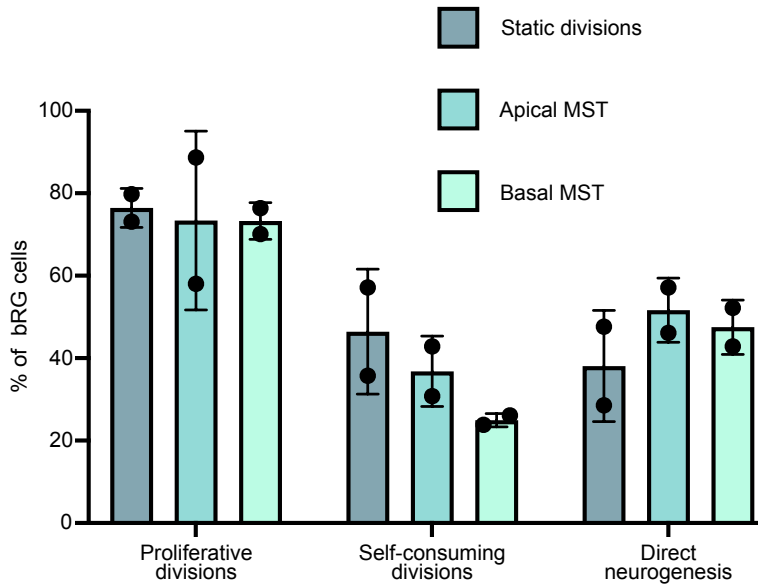
a



b



c

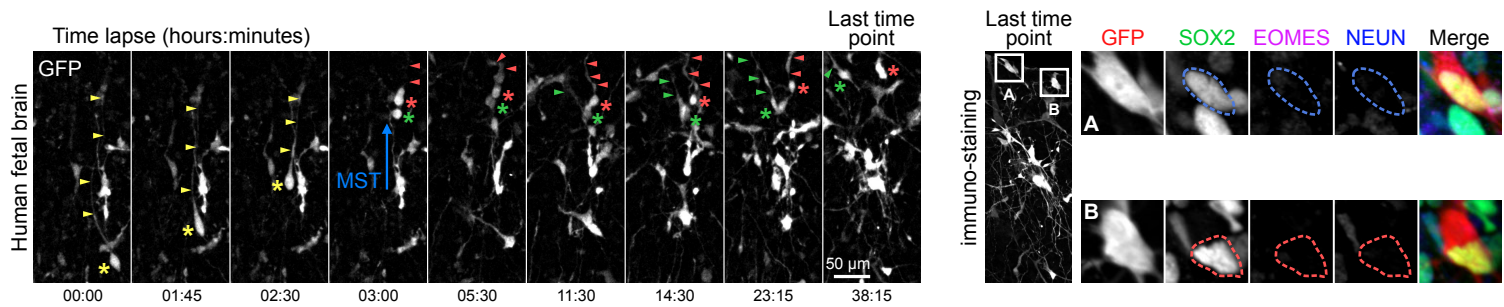


768 **Extended Data Fig. 5 Cell fate identification timing in fetal tissue.**

769 **a**, Live/fixed correlative analysis of a dividing bRG cell generating two bRG daughters. **b**,
770 Detection of bRG, IP or neuronal cell fate relative to the time of division of the bRG mother
771 cell in human fetal samples at GW 14-18. **c**, Percentage of bRG cells performing proliferative
772 divisions, of neurogenic bRG cells performing self-consuming divisions and of neurogenic
773 bRG cells performing direct neurogenic divisions, depending on their division mode (static,
774 apical MST or basal MST).

775

Figure S6

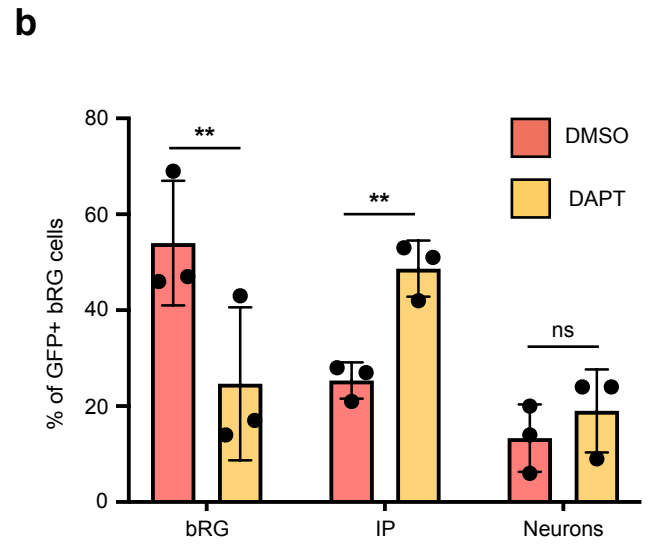
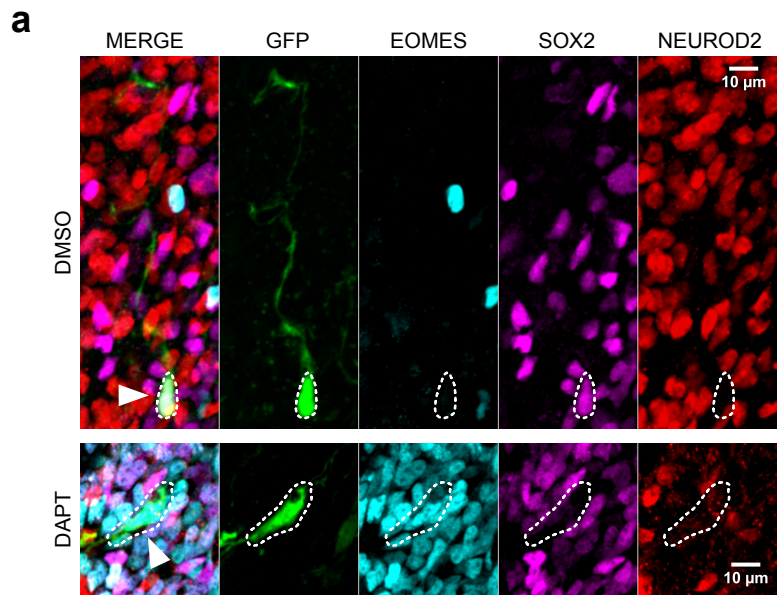


776 **Extended Data Fig. 6 SOX2+ bRG daughter cells regrow a basal process if at birth.**

777 **A.** Live/fixed correlative analysis of a dividing bRG cell generating two bRG daughters. Asterix
778 indicates cell soma and arrowhead indicates basal process. Mother cell (yellow) divides into a
779 process-inheriting cell (red) and a cell that regrows a basal process (green).

780

Figure S7



781 **Extended Data Fig. 7 NOTCH inhibition induces RG depletion and IP generation.**

782 **a**, Immunostaining for SOX2, EOMES and NEUROD2 in GFP-infected week 8 cerebral
783 organoids, following incubation with DMSO or 5 μ M DAPT for 48 hours. **b**. Percentage of bRG
784 (SOX2+), IPs (EOMES+) and Neurons (NEUROD2+) newborn GFP+ cells after 48 hour
785 treatment with DMSO or 5 μ M DAPT. All data are expressed as mean +/- standard deviation
786 (SD). **p<0,01, by two-tailed t-test.